POSITIVE FILTERED P_N MOMENT CLOSURES FOR LINEAR KINETIC EQUATIONS

M. PAUL LAIU*, CORY D. HAUCK†, RYAN G. MCCLARREN‡, DIANNE P. O'LEARY§, AND ANDRÉ L. TITS¶

Abstract. We propose a positive-preserving moment closure for linear kinetic transport equations based on a filtered spherical harmonic (FP_N) expansion in the angular variable. The recently proposed FP_N moment equations are known to suffer from the occurrence of (unphysical) negative particle concentrations. The origin of this problem is that the FP_N approximation is not always positive at the kinetic level; the new FP_N^+ closure is developed to address this issue. A new spherical harmonic expansion is computed via the solution of an optimization problem, with constraints that enforce positivity, but only on a finite set of pre-selected points. Combined with an appropriate PDE solver for the moment equations, this ensures positivity of the particle concentration at each step in the time integration. Under an additional, mild regularity assumption, we prove that as the moment order tends to infinity, the FP_N^+ approximation converges, in the L^2 sense, at the same rate as the FP_N approximation; numerical tests suggest that this assumption may not be necessary.

For purposes of comparison, we also consider a positive-preserving UD_N closure that is based on the uniform damping of coefficients in the FP_N approximation. While simple and less expensive to implement, the UD_N approximation does not converge as fast as the FP_N approximation for problems with limited regularity. We simulate the challenging line source benchmark problem with moment equations using several different choices of closure. The line source results indicate that, when compared to the UD_N closure, the accuracy of the FP_N^+ closure makes up for the overhead incurred by the optimization problem. In addition, we observe that for a regularized version of the line source problem, the UD_N closure causes severe degradation in the space-time convergence of the PDE solver, while the FP_N^+ closure does not.

1. Introduction. Kinetic transport equations are used to model particle-based systems in various areas including rarefied gases [8,9], radiative transport [12,31,40], and semiconductors [33]. These equations govern the evolution of a positive scalar function, the kinetic distribution, that depends on position, momentum, and time. In typical settings, the position-momentum phase space is six-dimensional. This makes the numerical simulation of these equations difficult.

Moment methods are commonly used to approximate the solution of kinetic equations. These methods track a finite number of moments (or weighted averages) of the kinetic distribution with respect to the momentum variable. Equations to describe the evolution of these moments are derived directly from the kinetic equation. However, for any finite number of moments, the exact moment equations are not closed, i.e., they require additional information about the kinetic distribution that is lost when

*Department of Electrical and Computer Engineering & Institute for Systems Research, University of Maryland College Park, MD 20742 USA, (mtlaiu@umd.edu). Supported by the U.S. Department of Energy, under Grant DESC0001862 and the SCGSR fellowship.

†Computational Mathematics Group, Computer Science and Mathematics Division, Oak Ridge National Laboratory, Oak Ridge, TN 37831 USA, (hauckc@ornl.gov). This author's research was sponsored by the Office of Advanced Scientific Computing Research and performed at the Oak Ridge National Laboratory, which is managed by UT-Battelle, LLC under Contract No. De-AC05-00OR22725.

‡Department of Nuclear Engineering, Texas A&M University, College Station, TX 77843, USA, (rgm@tamu.edu).

§Computer Science Department and Institute for Advanced Computer Studies, University of Maryland College Park, MD 20742 USA, (oleary@cs.umd.edu). Supported by the U.S. Department of Energy, under Grant DESC0001862.

¶Department of Electrical and Computer Engineering & Institute for Systems Research, University of Maryland College Park, MD 20742 USA, (andre@umd.edu). Supported by the U.S. Department of Energy, under Grant DESC0001862.

retaining only a finite number of moments. Hence a moment closure is needed to fill in the missing kinetic information and close the system of equations.

In this paper, we consider linear kinetic equations with a momentum variable that specifies the direction of particle travel by an angle on the unit sphere. In this setting, the most common moment closure method is the spherical harmonic approximation, or P_N method [7,31]. This method is equivalent to a standard spectral discretization of the kinetic equation with respect to the momentum variable. The finite expansion of the kinetic distribution in spherical harmonics provides the necessary closure, and the coefficients of the expansion are related to the tracked moments via a linear mapping.

Although computationally fast, the P_N method suffers from several well-known drawbacks. Like most spectral methods, it may produce highly oscillatory solutions that can lead to local negative values in the particle concentration.[1] Several moment closures have been proposed to address these issues. The M_N [5, 14, 22, 37] and PP_N [18, 23] closures were proposed to maintain the positivity of solutions by using a positive ansatz for the closure. This is in contrast to the spherical harmonic expansion for the P_N method, which may take on negative values. However, both the M_N and PP_N solutions are still quite oscillatory [18, 23] and much more expensive than P_N [1,2,17]. The recently proposed FP_N closure [34,42] still uses a spherical harmonics expansion, but damps the oscillations via a low pass filter on the moments. While the filter mitigates the occurrence of negative particle concentrations, they are not fully removed. Small negative values in the particle concentration may not hurt linear kinetic models, but for nonlinear models, negative concentrations may make the system unstable.[2] Hence, it is of interest to develop a positive-preserving[3] modification of the FP_N method.

In the current work, we propose a modification of the FP_N closure that preserves non-negativity on a finite, predetermined set of quadrature points. This set is part of a quadrature rule that is used to evaluate moments of the spherical harmonic expansion up to a given order exactly (up to machine precision). As shown in [2], this condition is sufficient to maintain a non-negative particle concentration. We refer to this new method as the FP_N^+ method.

Implementation of the FP_N^+ method requires a PDE solver to update the moment system in time and the solution of a constrained optimization problem to define the closure. For the PDE solver, we use the kinetic scheme developed in [2]; see also [18]. Meanwhile, the optimization problem can be written as a strictly convex quadratic program (CQP) with a large number of inequality constraints, which enforce positivity on the prescribed quadrature. We extend the constraint-reduced Mehrotra's predictor-corrector (MPC) linear program solver proposed in [44] to solve the CQPs that arise from the FP_N^+ method. The benefit of the constraint reduction technique increases with the number of quadrature points.

Further, the consistency properties of the FP_N^+ closure are analyzed in this paper. Under an additional, mild regularity assumption, we prove that as the moment order tends to infinity, the FP_N^+ approximation converges to the underlying target function, in the L^2 sense, as fast as the FP_N approximation. We then provide numerical results which suggest that this property holds even without the additional

[1] In this paper, we use the term "concentration" when referring to the integral of the kinetic distribution with respect to angle. The concentration is a function of position and time only.

[2] For example, when solving radiative transfer equations coupled with a material equation, the negative radiative energy-density can cause a negative material temperature [35, 39].

[3] In this paper, the term "positive-preserving" refers to methods that maintain the non-negativity of particle concentration.

assumption. For comparison, we also analyze and test the consistency properties of another positive-preserving closure that, for reasons that will become clear later, we refer to as the uniform damping (UD_N) closure. This closure was originally proposed in [32] to generate spatial reconstructions in the numerical simulation of hyperbolic conservation laws. More recently, it was applied to finite volume, weighted essentially non-oscillatory (WENO) and discontinuous Galerkin schemes in [46]. Because of its simplicity and fast implementation, the method has been applied in a variety of applications; see [47] for review and further references. We prove convergence results for the UD_N closure that are suboptimal when compared to the FP_N closure; numerical tests suggest that the estimates are likely sharp. For smooth problems, the difference in the accuracy of the closures is negligible. However, for problems with less regularity, the difference is substantial.

Finally, we compute the numerical solution from the FP_N^+ method on the line source benchmark problem [16] and compare it to solutions from the P_N, FP_N, PP_N, and UD_N methods. For the same number of moments, the FP_N^+ method performs much better than the UD_N method. However, enforcing positivity does create some local trade-offs in accuracy when compared to the FP_N method. The P_N and PP_N methods are not competitive. We also compare the efficiency of the more accurate FP_N^+ closure with the less expensive UD_N closure. In particular, we consider the solution time needed to reach a given level of accuracy in the particle concentration. For the line source problem, we conclude that the FP_N^+ solutions are generally two to ten times faster than the UD_N solutions to reach the same accuracy.

The remainder of the paper is organized as follows. In Section 2, we review the kinetic equation, moment equations, and several moment closures including P_N, FP_N, PP_N, and UD_N closures. Section 3 introduces the proposed FP_N^+ closure and illustrates the implementation details in the FP_N^+ method. In Section 4, the consistency analysis of the FP_N^+ and UD_N closures and numerical convergence results are provided. In Section 5, we present results for the line source problem. Section 6 is for conclusion and discussion.

2. Preliminaries and Notations.

2.1. Kinetic Equations and Moment Models. As in [18], we consider a linear kinetic model of particles traveling with unit speed[4] which scatter isotropically off of a background material medium. Emission, absorption, and external sources are neglected for simplifying the presentation; they can be included easily. The kinetic description is given by a non-negative distribution function $f = f(x, \Omega, t)$ where $x = (x_1, x_2, x_3) \in \mathbb{R}^3$ is the spatial position, $\Omega = (\Omega_1, \Omega_2, \Omega_3) \in \mathbb{S}^2$ is the direction of particle travel, and $t \geq 0$ is the time. In terms of the polar angle θ and the azimuthal angle ϕ, $(\Omega_1, \Omega_2, \Omega_3) = (\sin\theta\cos\phi, \sin\theta\sin\phi, \cos\theta)$. In what follows, it is often convenient to express functions on $\mathbb{S}^2$ in terms $\mu := \cos\theta$ and ϕ.

The governing linear kinetic equation is of the form

$$\partial_t f + \Omega \cdot \nabla_x f = \frac{\sigma}{4\pi}\langle f \rangle - \sigma f\,, \tag{2.1}$$

where σ is the scattering cross-section, and the angle brackets denote integration with respect to Ω over the angular space $\mathbb{S}^2$, i.e., $\langle f \rangle(x,t) = \int_{\mathbb{S}^2} f(x, \Omega, t)\, d\Omega$. To obtain a unique solution, one must equip (2.1) with appropriate initial and boundary conditions.

[4]The unit speed assumption reduces the problem from six dimensions to five.

Moments $\mathbf{u}^f$ associated to f are defined as

$$\mathbf{u}^f = \mathbf{u}^f(x,t) := \langle \mathbf{m} f(x,\cdot,t)\rangle \,, \tag{2.2}$$

where $\mathbf{m}$ is a vector of basis functions over $\mathbb{S}^2$. Following standard practice, we use spherical harmonic basis functions.[5] For moments up to order N, the spherical harmonics basis $\mathbf{m} : \mathbb{S}^2 \to \mathbb{R}^n$, $n = (N+1)^2$, is given by $\mathbf{m} = [m_0; \mathbf{m}_1; \dots; \mathbf{m}_N]$, where $\mathbf{m}_\ell$ is the collection of the $2\ell+1$ harmonics of degree ℓ, which are defined explicitly in [18]. The components of $\mathbf{m}$ form an orthogonal basis for $\mathbb{P}_N(\mathbb{S}^2)$, the space of polynomials in Ω on $\mathbb{S}^2$ with degree at most N. We assume the components of $\mathbf{m}$ are normalized so that $\langle \mathbf{m}\mathbf{m}^T\rangle = I_{n\times n}$.

Equations for $\mathbf{u}^f$ are derived by multiplying the kinetic equation (2.1) by $\mathbf{m}$ and integrating over $\mathbb{S}^2$, which gives

$$\partial_t \mathbf{u}^f + \nabla_x \cdot \langle \mathbf{m}\Omega f\rangle = -\sigma R \mathbf{u}^f, \tag{2.3}$$

where the $n \times n$ matrix $R = \operatorname{diag}(0, 1, \dots, 1)$. Equation (2.3) is exact, but it is not closed due to the flux term $\langle \mathbf{m}\Omega f\rangle$. Specifically, the spherical harmonic expansion of $\mathbf{m}_N \Omega$ involves harmonics of degree $N+1$ so that $\langle \mathbf{m}\Omega f\rangle$ cannot be expressed as a function of $\mathbf{u}^f$.

In order to close (2.3), we define an operator $\mathcal{E} : \mathbb{R}^n \to L^2(\mathbb{S}^2)$ that maps a given set of moments to a distribution on $\mathbb{S}^2$ that approximates f. Then (2.3) can be closed by substituting the *ansatz* $\mathcal{E}[\mathbf{u}]$ for f, which yields the closed moment system

$$\partial_t \mathbf{u} + \nabla_x \cdot \langle \mathbf{m}\Omega \mathcal{E}[\mathbf{u}]\rangle = -\sigma R \mathbf{u} \,. \tag{2.4}$$

The solution $\mathbf{u} = [u_0; \mathbf{u}_1; \dots; \mathbf{u}_N]$ of system (2.4) is an approximation of the exact moments $\mathbf{u}^f$. Equation (2.4) can be solved numerically in a variety of ways. In this paper, we use the kinetic scheme proposed in [2,18]; the full description of the scheme is included in the supplementary materials.

In slab geometry, the distribution f in (2.1) is independent of x_1 and x_2, i.e., $\partial_{x_1} f = \partial_{x_2} f = 0$. Thus one can express the angular dependence of f in terms of $\mu = \Omega_3$ only, thereby reducing the angular domain from $\mathbb{S}^2$ to $[-1, 1]$.[6] Thus, we consider also in the paper convergence of the FP_N^+ closure on the interval $[-1, 1]$. In this case, the angle brackets denote integration with respect to $\mu \in [-1, 1]$, and the moment basis $\mathbf{m} : [-1, 1] \to \mathbb{R}^n$, $n = N+1$, is given by $\mathbf{m} = [m_0; m_1; \dots; m_N]$, where m_ℓ is the ℓ-th order Legendre polynomial on μ. The components of $\mathbf{m}$ in this case form an orthogonal basis for $\mathbb{P}_N([-1, 1])$, the vector space of polynomials on $[-1, 1]$ of degree at most N. We assume the standard normalization $\langle m_\ell^2\rangle = \frac{2}{2\ell+1}$. Note that (2.3) and (2.4) still hold true for slab geometry, with the modified angular space and moment basis.

In the remaining parts of Section 2 and Section 3, we present several moment closures in full geometry. These closures can be formulated analogously in the case of slab geometry with minor modifications, as described in the preceding paragraph.

2.2. P_N Closures. The P_N equations approximate the linear kinetic equation (2.1) via a standard spectral method. For $\mathbf{u} \in \mathbb{R}^n$, the P_N operator $\mathcal{E}_{\mathrm{P}_N} : \mathbb{R}^n \to$

[5] Spherical harmonics are eigenfunctions of general scattering operators. See, for example, [31, Section 1-4].

[6] In spherically symmetric geometries, the effective angular space also reduces to $[-1, 1]$, (See, for example, details in [40, Chapter 5].)

$\mathbb{P}_N(\mathbb{S}^2)$ maps moments $\mathbf{u}$ to $\mathbb{P}_N(\mathbb{S}^2)$, with

$$\mathcal{E}_{\mathrm{P}_N}[\mathbf{u}] := \hat{\boldsymbol{\alpha}}_{\mathrm{P}_N}(\mathbf{u})^T \mathbf{m}\,, \tag{2.5}$$

where the P_N ansatz $\mathcal{E}_{\mathrm{P}_N}[\mathbf{u}]$ solves the L^2 entropy minimization problem

$$\underset{g \in L^2}{\text{minimize}} \quad \frac{1}{2}\left\langle g^2 \right\rangle \quad \text{subject to} \quad \langle \mathbf{m} g \rangle = \mathbf{u}\,, \tag{2.6}$$

and the expansion coefficients $\hat{\boldsymbol{\alpha}}_{\mathrm{P}_N}(\mathbf{u})$ solve the dual problem of (2.6), and are given by

$$\hat{\boldsymbol{\alpha}}_{\mathrm{P}_N}(\mathbf{u}) := \underset{\boldsymbol{\alpha} \in \mathbb{R}^n}{\operatorname{argmin}} \left\{ \frac{1}{2}\left\langle |\boldsymbol{\alpha}^T \mathbf{m}|^2 \right\rangle - \mathbf{u}^T \boldsymbol{\alpha} \right\} = \langle \mathbf{m}\mathbf{m}^T \rangle^{-1} \mathbf{u} = \mathbf{u}\,. \tag{2.7}$$

Setting $\mathcal{E}[\mathbf{u}] = \mathcal{E}_{\mathrm{P}_N}[\mathbf{u}]$ in (2.4) gives the P_N equations:

$$\partial_t \mathbf{u} + \nabla_x \cdot \left\langle \Omega \mathbf{m}\mathbf{m}^T \right\rangle \mathbf{u} = -\sigma R \mathbf{u}\,. \tag{2.8}$$

2.3. Filtered P_N Closures (FP_N). Filtering is commonly used to mitigate Gibbs phenomena in spectral methods for the spatial discretization of hyperbolic problems [20, 21]. Filtered spherical harmonics expansions for angular moment closures were first proposed in [34] in order to suppress oscillations and mitigate the occurrence of negative concentrations in the P_N solution.

The filter can be embedded directly into the numerical PDE solver for the P_N equations (2.8): before each time step, the moment $\mathbf{u}$ is replaced by $F\mathbf{u}$ where $F = \operatorname{blockdiag}(F_\ell I_{(2\ell+1)\times(2\ell+1)})$ is an $n \times n$ matrix and each $F_\ell \in [0,1]$ is a filtering coefficient, with $F_0 = 1$. Associated to $F\mathbf{u}$ is the ansatz

$$\mathcal{E}_{\mathrm{FP}_N}[\mathbf{u}] := \mathcal{E}_{\mathrm{P}_N}[F\mathbf{u}] = \hat{\boldsymbol{\alpha}}_{\mathrm{FP}_N}(\mathbf{u})^T \mathbf{m}\,, \tag{2.9}$$

where $\hat{\boldsymbol{\alpha}}_{\mathrm{FP}_N}(\mathbf{u}) := \hat{\boldsymbol{\alpha}}_{\mathrm{P}_N}(F\mathbf{u})$ solves the filtered version of dual problem (2.7)

$$\hat{\boldsymbol{\alpha}}_{\mathrm{FP}_N}(\mathbf{u}) = \underset{\boldsymbol{\alpha} \in \mathbb{R}^n}{\operatorname{argmin}} \left\{ \frac{1}{2}\left\langle |\boldsymbol{\alpha}^T \mathbf{m}|^2 \right\rangle - (F\mathbf{u})^T \boldsymbol{\alpha} \right\} = F\hat{\boldsymbol{\alpha}}_{\mathrm{P}_N}(\mathbf{u})\,. \tag{2.10}$$

We call this the *discrete embedding* of the filter.

The original choice of F_ℓ in [34] was based on an optimization problem that penalizes angular derivatives of the ansatz. In [42], a more general formulation leads to a modified system of equations. There F_ℓ is given by

$$F_\ell = \left[\kappa\left(\frac{\ell}{N+1}\right)\right]^\nu\,, \quad \text{where} \quad \nu = -\frac{\sigma_{\mathrm{F}} \Delta t}{\log[\kappa(N/(N+1))]} \tag{2.11}$$

depends on the time step, σ_{F} is a tuning parameter, and $\kappa : \mathbb{R}^+ \to [0,1]$ is a filter function. We say κ has order $p > 0$ if $\kappa \in C^p(\mathbb{R}^+)$ and $\kappa(0) = 1$ and $\kappa^{(k)}(0) = 0$ for $k = 1, \ldots, p-1$.

The choice of ν in (2.11) ensures the discrete embedding is formally consistent in the limit $\Delta t \to 0$ with a modified version of (2.8), the FP_N equations:

$$\partial_t \mathbf{u}^* + \nabla_x \cdot \left\langle \Omega \mathbf{m}\mathbf{m}^T \right\rangle \mathbf{u}^* = -\sigma R \mathbf{u}^* - \sigma_{\mathrm{F}} L \mathbf{u}^*\,, \tag{2.12}$$

where $L = \operatorname{blockdiag}(L_\ell I_{(2\ell+1)\times(2\ell+1)})$, and $L_\ell = \frac{\log\left(\kappa\left(\frac{\ell}{N+1}\right)\right)}{\log\left(\kappa\left(\frac{N}{N+1}\right)\right)}$. We refer to (2.12) as a *continuous embedding* of the filter.

In the following sections, we consider both types of embeddings: discrete and continuous. The discrete approach is more conducive to the consistency analysis in Section 4, while the continuous approach is better for assessing the space-time convergence of the PDE solver in Section 3.2.1. In Section 4.2, the convergence results of the FP_N closures are presented for the 2nd-order Lanczos filter [42], 4th-order spherical spline filter [42], and the 6th-order exponential filter [15]. The filter functions κ are given by

$$\kappa_{\mathrm{Lanczos}}(\eta) = \frac{\sin(\eta)}{\eta}\,, \quad \kappa_{\mathrm{SSpline}}(\eta) = \frac{1}{1+\eta^4}\,, \quad \kappa_{\mathrm{Exp}}(\eta) = \exp(c\eta^6)\,, \tag{2.13}$$

where, in the definition of κ_{Exp}, $c = \log(\epsilon_M)$, ϵ_M being the machine precision. In the numerical tests presented in Section 5.2, the 4th-order spherical spline filter is used.

While the FP_N closure effectively damps oscillations in the numerical solution, it still suffers from some challenges. These include (i) the occurrence of negative particle concentrations that can affect the stability of nonlinear systems (see [35, 39]) and (ii) the lack of a systematic way to choose the tuning parameter σ_{F}. In the remainder of this paper, we address the former.

2.4. Positive $\mathbf{P}_N$ Closures ($\mathbf{PP}_N$). In [23], a positive particle concentration is ensured imposing point-wise positivity constraints on a discretized version of (2.6). Let $\mathcal{Q}$ and $\mathcal{W}$ be the points and (strictly positive) weights of a quadrature rule on $\mathbb{S}^2$ with degree of precision $2N+1$—that is, the quadrature rule integrates polynomials in $\mathbb{P}_{2N+1}(\mathbb{S}^2)$ exactly (in exact arithmetic). Then the discrete PP_N ansatz $\mathcal{E}_{\mathrm{PP}_N} : \mathbb{R}^n \to \mathbb{R}^{|\mathcal{Q}|}$ maps $\mathbf{u}$ to the unique minimizer for

$$\begin{aligned} \underset{g\in\mathbb{R}^{|\mathcal{Q}|}}{\text{minimize}} \quad & \frac{1}{2}\sum_{k=1}^{|\mathcal{Q}|} w_k |g_k|^2 \\ \text{subject to} \quad & \sum_{k=1}^{|\mathcal{Q}|} w_k \mathbf{m}(\Omega_k) g_k = \mathbf{u}\,, \\ & g_k \geq 0\,, \quad \forall k \in \{1,\dots,|\mathcal{Q}|\}\,, \end{aligned} \tag{2.14}$$

where $(\Omega_k, w_k) \in (\mathcal{Q}, \mathcal{W})$ for all $k \in \{1,\dots,|\mathcal{Q}|\}$. If $\mathcal{E}_{\mathrm{P}_N}[\mathbf{u}] \geq 0$ on $\mathcal{Q}$, then $\mathcal{E}_{\mathrm{PP}_N}[\mathbf{u}]$ is just the restriction of $\mathcal{E}_{\mathrm{P}_N}[\mathbf{u}]$ to $\mathcal{Q}$.

In [18], a continuum variant of the PP_N closure was proposed to enforce positivity by adding a log penalty term to (2.6). In this case, the PP_N operator $\mathcal{E}_{\mathrm{PP}_N} : \mathbb{R}^n \to L^2(\mathbb{S}^2)$ maps $\mathbf{u}$ to the unique minimizer for

$$\underset{g\in L^2(\mathbb{S}^2)}{\text{minimize}} \ \left\langle \frac{1}{2}g^2 - \delta \log g \right\rangle \qquad \text{subject to} \ \langle \mathbf{m} g\rangle = \mathbf{u}\,, \tag{2.15}$$

where $\delta > 0$ is a penalty parameter. Although (2.15) is formulated as a continuous problem, a quadrature rule is still required to approximate the integrals in the objective.

While both variants (2.14) and (2.15) of the PP_N closures generate a positive ansatz, numerical solutions of the modified optimization problems (2.14) and (2.15) are significantly more expensive to obtain. Moreover, neither ansatz is a polynomial. A consequence of this is that solutions of the PP_N equations suffer from artifacts, known as *ray effects* [31, Section 4-6], due to the fact that the quadrature rule is not exact.

2.5. Uniform Damping Closures (UD_N). Uniform damping (UD) is a simple method for generating a non-negative polynomial reconstruction from given moments. It was first proposed in [32] as a limiter for finite volume discretizations of hyperbolic PDE, and has recently been used to generate discontinuous Galerkin and finite volume WENO methods [46, 47] that satisfy maximum principles while maintaining high-order.

The UD_N closure is a simple application of the UD method. It works by damping moments $\mathbf{u}_\ell$ uniformly for all $\ell > 0$, while preserving u_0. Given quadrature points and weights $(\mathcal{Q}, \mathcal{W})$, the UD_N operator $\mathcal{E}_{\mathrm{UD}_N} : \mathbb{R}^n \to \mathbb{P}_N(\mathbb{S}^2)$ maps $\mathbf{u}$ to the ansatz

$$\mathcal{E}_{\mathrm{UD}_N}[\mathbf{u}] := \frac{u_0}{u_0 + \langle m_0 c_N \rangle}(\mathcal{E}_{\mathrm{FP}_N}[\mathbf{u}] + c_N), \quad c_N = -\min\left\{\min_{\Omega_k \in \mathcal{Q}} \mathcal{E}_{\mathrm{FP}_N}[\mathbf{u}](\Omega_k), 0\right\}. \tag{2.16}$$

This ansatz is still a spherical harmonics expansion; hence UD_N solutions do not suffer from ray effects as PP_N solutions do. In addition, it is inexpensive to implement. However, as proved in Theorem 4.4 in Section 4.1 and shown in Section 5.2, the UD_N closure may lose accuracy for problems with non-smooth solutions.

3. Positive Filtered P_N Closures (FP_N^+). To overcome the drawbacks of the FP_N, PP_N, and UD_N closures, we design *positive filtered* P_N (or FP_N^+) closures. This closure prevents the occurrence of negative particle concentrations using a polynomial ansatz that is non-negative at a pre-selected set of quadrature points. The FP_N^+ ansatz is defined via the solution of an optimization problem. The FP_N^+ ansatz is more expensive to compute than the UD_N ansatz; however, it is more accurate. The benefits of this additional accuracy are analyzed and explored in Sections 4 and 5.

3.1. Formulation. The FP_N^+ operator $\mathcal{E}_{\mathrm{FP}_N^+} : \mathbb{R}^n \to \mathbb{P}_N(\mathbb{S}^2)$ maps moments $\mathbf{u}$ to the ansatz

$$\mathcal{E}_{\mathrm{FP}_N^+}[\mathbf{u}] := \hat{\boldsymbol{\alpha}}_{\mathrm{FP}_N^+}(\mathbf{u})^T \mathbf{m}\,, \tag{3.1}$$

where $\hat{\boldsymbol{\alpha}}_{\mathrm{FP}_N^+}(\mathbf{u})$ solves

$$\begin{aligned} \underset{\boldsymbol{\alpha} \in \mathbb{R}^n}{\text{minimize}} \quad & \frac{1}{2}\|\boldsymbol{\alpha}^T \mathbf{m} - \mathcal{E}_{\mathrm{FP}_N}[\mathbf{u}]\|^2_{L^2(\mathbb{S}^2)} \\ \text{subject to} \quad & \boldsymbol{\alpha}^T \mathbf{m}(\Omega_k) \geq 0\,, \quad \forall \Omega_k \in \mathcal{Q}\,, \\ & \left\langle m_0 \boldsymbol{\alpha}^T \mathbf{m} \right\rangle = u_0\,, \end{aligned} \tag{3.2}$$

and $\mathcal{Q}$ is a quadrature set. The FP_N^+ ansatz is the best L^2 approximation to the FP_N ansatz in $\mathbb{P}_N(\mathbb{S}^2)$ that is non-negative on $\mathcal{Q}$ and preserves particle concentration.[7] The set $\mathcal{Q}$ is chosen so that the associated quadrature rule has degree of precision $2N+1$. This implies that the flux term $\langle \Omega \mathbf{m} \mathcal{E}[\mathbf{u}] \rangle$ in (2.4) is evaluated exactly whenever $\mathcal{E}[\mathbf{u}] \in \mathbb{P}_N(\mathbb{S}^2)$. It also ensures that u_0 is non-negative in the next update of the PDE solver (see Section 3.2.1 and the supplementary materials for details).

Like the standard filter, the positive-preserving filter (3.2) can be discretely embedded into the numerical PDE solver for the P_N equations (2.8)[8]: before each time step, the moment $\mathbf{u}$ is replaced by $\langle \mathbf{m} \mathcal{E}_{\mathrm{FP}_N^+}[\mathbf{u}] \rangle$. If the inequality constraints in (3.2) are not active at the solution, then $\langle \mathbf{m} \mathcal{E}_{\mathrm{FP}_N^+}[\mathbf{u}] \rangle = F\mathbf{u}$. Indeed, in this case, (3.2) is

[7] The scalar u_0 is a positive constant multiple of the particle concentration.
[8] See the discussion on discrete and continuous embeddings in Section 2.3.

equivalent to the dual problem in (2.10). When the inequality constraints are active, $\langle \mathbf{m}\mathcal{E}_{\mathrm{FP}_N^+}[\mathbf{u}]\rangle$ depends on $\mathbf{u}$ in a nonlinear way that cannot be expressed in closed form. Rather it must be determined from the numerical solution of (3.2). With the continuous embedding, the filter is built in to the equations, but positivity is still embedded in the numerics: at each time step of the numerical PDE solver for the FP_N equations (2.12), the moment $\mathbf{u}^*$ is replaced by $\langle \mathbf{m}\mathcal{E}_{\mathrm{P}_N^+}[\mathbf{u}^*]\rangle$ where $\mathcal{E}_{\mathrm{P}_N^+}$ is given by (3.1) when there is no filter—that is, when $F = I$.

3.2. Implementation. In this subsection, we summarize the implementation of the FP_N^+ closures, which includes a numerical PDE solver for (2.4) and an algorithm for the optimization problem (3.2). Further details can be found in the supplementary materials.

3.2.1. Numerical PDE Solver. We generate a numerical solution of the FP_N^+ equations using a second-order kinetic scheme that was developed in [2]. (See references therein for early developments of this type of method.) The scheme is based on the following discrete ordinate approximation of (2.1):

$$\partial_t f^{\mathcal{Q}} + \nabla_x \cdot \Omega f^{\mathcal{Q}} = \frac{\sigma}{4\pi}\langle f^{\mathcal{Q}}\rangle_{\mathcal{Q}} - \sigma f^{\mathcal{Q}} , \tag{3.3}$$

where $f^{\mathcal{Q}}(x,\Omega,t) \approx f(x,\Omega,t)$ for each ordinate Ω in a quadrature set $\mathcal{Q}$ and $\langle\cdot\rangle_{\mathcal{Q}}$ denotes the quadrature rule associated to $\mathcal{Q}$. With an appropriate choice of quadrature, the P_N equations (2.8) can be derived directly from (3.3). Indeed, by taking quadrature-based moments of (3.3) and using the ansatz $\mathcal{E}_{\mathrm{P}_N}[\mathbf{u}]$ to approximate $f^{\mathcal{Q}}$, we arrive at the following system for the unknowns $\mathbf{u}$:

$$\partial_t\langle \mathbf{m}\mathcal{E}_{\mathrm{P}_N}[\mathbf{u}]\rangle_{\mathcal{Q}} + \nabla_x \cdot \langle \Omega\mathbf{m}\mathcal{E}_{\mathrm{P}_N}[\mathbf{u}]\rangle_{\mathcal{Q}} = \frac{\sigma}{4\pi}\langle \mathbf{m}\rangle_{\mathcal{Q}}\langle \mathcal{E}_{\mathrm{P}_N}[\mathbf{u}]\rangle_{\mathcal{Q}} - \sigma\langle \mathbf{m}\mathcal{E}_{\mathrm{P}_N}[\mathbf{u}]\rangle_{\mathcal{Q}} . \tag{3.4}$$

If, as in Section 3.1, the quadrature set $\mathcal{Q}$ is chosen so that $\langle\cdot\rangle_{\mathcal{Q}}$ has degree of precision $2N+1$, then (3.4) is equivalent to (2.8). This is our motivation for the choice of quadrature. A similar procedure can also be used to update the FP_N equations in (2.12).

It is known [2] that with an appropriate CFL condition, a finite volume discretization of (3.3) preserves the positivity of $f^{\mathcal{Q}}$. The corresponding kinetic scheme for (3.4) is derived by taking quadrature moments of this discretization and thus preserves positivity of the particle concentration. Details of this scheme and a precise statement of the positivity result are given in the supplementary materials.

3.2.2. Solving the FP_N^+ Optimization Problem. If $\hat{\boldsymbol{\alpha}}_{\mathrm{FP}_N}(\mathbf{u})$ satisfies the non-negativity constraints in (3.2), then $\hat{\boldsymbol{\alpha}}_{\mathrm{FP}_N}(\mathbf{u})$ solves (3.2)—that is, $\hat{\boldsymbol{\alpha}}_{\mathrm{FP}_N^+}(\mathbf{u}) = \hat{\boldsymbol{\alpha}}_{\mathrm{FP}_N}(\mathbf{u})$. Otherwise, a numerical optimization algorithm is needed. We discuss such an algorithm here.

Due to the orthonormality of spherical harmonics, the equality constraint $\left\langle m_0\boldsymbol{\alpha}^T\mathbf{m}\right\rangle = u_0$ in (3.2) is equivalent to $\alpha_0 = u_0$. Hence the variable α_0 can be removed from the minimization problem, and (3.2) can be rewritten as

$$\begin{aligned} \underset{\tilde{\boldsymbol{\alpha}}\in\mathbb{R}^{n-1}}{\text{minimize}} \quad & \frac{1}{2}\left\langle|\tilde{\boldsymbol{\alpha}}^T\tilde{\mathbf{m}}|^2\right\rangle - (\tilde{F}\tilde{\mathbf{u}})^T\tilde{\boldsymbol{\alpha}} \\ \text{subject to} \quad & \tilde{\boldsymbol{\alpha}}^T\tilde{\mathbf{m}}(\Omega_k) \geq -m_0u_0 , \qquad \forall\Omega_k\in\mathcal{Q} , \end{aligned} \tag{3.5}$$

where $\tilde{\boldsymbol{\alpha}} = [\alpha_1,\dots,\alpha_{n-1}]^T$, and similarly for $\tilde{\mathbf{u}}$, $\tilde{\mathbf{m}}$, and $\tilde{F}$. This is a convex quadratic program (CQP), which can be solved using primal-dual interior-point methods, including affine-scaling (AS) [45] and Mehrotra's predictor-corrector (MPC) approach [36].

Because the main computational cost (per iteration) of standard interior-point methods is proportional to the number of constraints, constraint-reduced variants of these algorithms are preferred. Constraint reduction for the AS algorithm was developed in [24]. Details of our version of the constraint-reduced MPC algorithm are provided in the supplementary materials. For the test problem in Section 5, we find that the MPC algorithm performs better than the AS algorithm; and in both cases, constraint reduction provides additional efficiency, particularly for larger quadrature sets.

3.2.3. Quadrature. We use two types of quadrature to define the FP_N^+ and UD_N closures and evaluate the numerical flux in the PDE solver. One of them is a product quadrature on the unit sphere [3, 43]. For closures with moment order N, we require the quadrature to have degree of precision $2N+1$, so we need a grid of at least $N+1$ (or $(N+1)/2$, for even functions on μ) Gauss-Legendre points in the μ direction and $2(N+1)$ equally spaced points in the ϕ direction.

Another quadrature we use is the Lebedev quadrature [26–30], which requires fewer quadrature points than the product quadrature does to achieve the same degree of precision. This property significantly reduces the computation time of the FP_N^+ method, where the quadrature points are not only used in numerical integration, but also involved in the formulation of the optimization problem (3.5). Some comparisons of these two types of quadrature are given in Table 5.1, and discussed in Remark 4.

4. Consistency Results. In this section, we analyze consistency properties of the FP_N^+ and UD_N approximations and report numerical convergence results, for both full and slab geometries. We consider target functions $\Psi = \Psi(\mu, \phi)$ where $\mu = \Omega_3 \in [-1, 1]$ and $\phi \in [0, 2\pi]$ is the azimuthal angle on the sphere, and functions $\psi = \psi(\mu)$ which correspond to the slab geometry case discussed in Section 2.1.

For $q \in \mathbb{R}$, the fractional Sobolev spaces $H^q([-1, 1])$ is the set of functions ψ such that the norm

$$\|\psi\|_{H^q([-1,1])} := \left(\sum_{\ell=0}^{\infty} \ell^q (1+\ell)^q \left(\frac{2\ell+1}{2} \right) |\alpha_\ell|^2 \right)^{1/2}, \quad \alpha_\ell = \int_{-1}^{1} \psi(\mu) m_\ell(\mu) d\mu \tag{4.1}$$

is finite [38]. In this definition, m_ℓ is the ℓ^{th} Legendre polynomial. The space $H^q(\mathbb{S}^2)$ is the set of functions ψ such that the norm

$$\|\psi\|_{H^q(\mathbb{S}^2)} := \left(\sum_{\ell=0}^{\infty} \sum_{|j| \le \ell} \ell^q (1+\ell)^q |\alpha_\ell^j|^2 \right)^{1/2}, \quad \alpha_\ell^j = \int_{\mathbb{S}^2} \psi(\Omega) m_\ell^j(\Omega) d\Omega \tag{4.2}$$

is finite [21]. In this definition, m_ℓ^j is the degree ℓ, order j spherical harmonic. In the remainder of this section, we use $\mathcal{S}$ to denote either $[-1, 1]$ or $\mathbb{S}^2$. Recall that $H^0(\mathcal{S}) = L^2(\mathcal{S})$.

For $q > 0$, let $q = v + w$, v a positive integer and $w \in [0, 1)$. Then the space $C^q([-1, 1])$ is defined as the set of functions ψ such that the norm

$$\|\psi\|_{C^q([-1,1])} := \|\psi\|_{L^\infty([-1,1])} + \sup_{\substack{\mu_1,\mu_2 \in [-1,1] \\ \mu_1 \neq \mu_2}} \frac{|\psi^{(v)}(\mu_1) - \psi^{(v)}(\mu_2)|}{|\mu_1 - \mu_2|^w} \tag{4.3}$$

is finite [38]. Here $\psi^{(v)}$ is the v-th strong derivative of ψ on $[-1, 1]$. Similarly, the space $C^q(\mathbb{S}^2)$ is defined as the set of functions ψ such that the norm

$$\|\psi\|_{C^q(\mathbb{S}^2)} := \|\psi\|_{L^\infty(\mathbb{S}^2)} + \max_{1\le i<j\le 3} \sup_{0<|\vartheta|\le 1} \frac{\|(I - R_{i,j,\vartheta})D^v_{i,j}\psi\|_{L^\infty(\mathbb{S}^2)}}{|\vartheta|^w}\,, \tag{4.4}$$

is finite [11]. Here the operator $D_{i,j} := x_i\partial_{x_i} - x_j\partial_{x_j}$, x_1, x_2, x_3 are the Cartesian coordinates on the sphere, I denotes the identity operator, and $R_{i,j,\vartheta}$ denotes the rotation operator such that $R_{i,j,\vartheta}g(\Omega) = g(\Omega')$, where Ω' is obtained by rotating Ω with angle ϑ in the x_i-x_j plane. Note that, for $q \in \mathbb{N}$, the space $C^q(\mathcal{S})$ is the space of functions with a continuous q-th derivative on $\mathcal{S}$. Finally, recall that $C^q(\mathcal{S}) \subset H^q(\mathcal{S})$.

4.1. Error Estimates of approximations. The P_N approximation (2.5) is based on the degree N spherical harmonic expansion of $\psi \in L^2(\mathbb{S}^2)$ with moments $\mathbf{u}^N := \mathbf{u}$.[9] For $\psi \in C^\infty(\mathbb{S}^2)$, this expansion converges to ψ (in the L^2 sense) faster than any negative power of N. For $\psi \in H^q(\mathbb{S}^2)$, it converges to ψ (in the L^2 sense) at rate q [10]. The filtered expansion (2.9) shares the convergence rate q with the P_N approximation if the filter order p satisfies $p \ge q$, but has a slower convergence rate p otherwise; see [15]. Based on these results, we establish the following convergence properties for the FP_N^+ approximation.

Theorem 4.1. *For $M > 0$, let $\mathcal{D}_M = \{g \in L^\infty(\mathcal{S}) : \|g\|_{L^\infty(\mathcal{S})} \le M\|g\|_{L^1(\mathcal{S})}\}$. Then, given a non-negative function $\psi \in C^q(\mathcal{S}) \cap \mathcal{D}_M$, $q \ge 0$, there exists a constant $A(q, M)$ such that*

$$\|\psi - \mathcal{E}_{FP_N^+}[\mathbf{u}^N]\|_{L^2(\mathcal{S})} \le A(q, M)N^{-s}\|\psi\|_{C^q(\mathcal{S})}, \quad \forall N \in \mathbb{N}\,, \tag{4.5}$$

where $\mathbf{u}^N \in \mathbb{R}^n$ consists of the moments of ψ up to order N, and $s = \min\{q, p\}$, with p the order of filter F in (2.10).

Before proving Theorem 4.1, we give two lemmas which are used in the proof. The first lemma gives the convergence rate of the FP_N approximation, and the second lemma provides an L^∞ error estimate of the best polynomial approximation for continuous functions.

Lemma 4.2. *For every $q \in \mathbb{R}$, there exists a constant $A_1(q)$ such that, for all $\psi \in H^q(\mathcal{S})$,*

$$\|\psi - \mathcal{E}_{FP_N}[\mathbf{u}^N]\|_{L^2(\mathcal{S})} \le A_1(q)N^{-s}\|\psi\|_{H^q(\mathcal{S})}, \quad \forall N \in \mathbb{N}\,, \tag{4.6}$$

where $\mathbf{u}^N \in \mathbb{R}^n$ consists of the moments of ψ up to order N, and $s = \min\{q, p\}$, with p the filter order in (2.10).

Proof. See [15]. □

Lemma 4.3. *For every $q \ge 0$, there exists a constant $A_2(q)$ such that, for all $\psi \in C^q(\mathcal{S})$,*

$$\min_{\varphi\in\mathbb{P}_N(\mathcal{S})} \|\psi - \varphi\|_{L^\infty(\mathcal{S})} \le A_2(q)N^{-q}\|\psi\|_{C^q(\mathcal{S})}, \quad \forall N \in \mathbb{N}\,, \tag{4.7}$$

where the minimum is attained.

Proof. From [41, Theorem 2] (for $\mathcal{S} = [-1, 1]$) and [11, Theorem 4.8.1] (for $\mathcal{S} = \mathbb{S}^2$)

$$\inf_{\varphi\in\mathbb{P}_N(\mathcal{S})} \|\psi - \varphi\|_{L^\infty(\mathcal{S})} \le A_2(q)N^{-q}\|\psi\|_{C^q(\mathcal{S})}\,. \tag{4.8}$$

[9] In this section, we use a superscript to emphasize the dependence of the moment vector on N.

Since $\mathbb{P}_N(\mathcal{S})$ is a finite dimensional subspace of the Banach space $C^q(\mathcal{S})$, it follows from Theorem 1.1 in [13] that the infimum in (4.8) is attained. $\square$

We now prove Theorem 4.1 for the case $\mathcal{S} = \mathbb{S}^2$; when $\mathcal{S} = [-1, 1]$, the result can be proved analogously. To simplify notation, we write

$$\|\cdot\|_{C^q} = \|\cdot\|_{C^q(\mathbb{S}^2)}\,; \quad \|\cdot\|_{L^p} = \|\cdot\|_{L^p(\mathbb{S}^2)}\,; \quad \mathcal{E}_{\mathrm{FP}_N} = \mathcal{E}_{\mathrm{FP}_N}[\mathbf{u}^N]\,; \quad \mathcal{E}_{\mathrm{FP}_N^+} = \mathcal{E}_{\mathrm{FP}_N^+}[\mathbf{u}^N]. \tag{4.9}$$

Proof of Theorem 4.1. If $\psi = 0$, then $\mathbf{u}^N = 0$ and $\mathcal{E}_{\mathrm{FP}_N^+} = 0$, and the claim holds trivially. Hence consider the case for $\psi \neq 0$, i.e., $\langle \psi \rangle > 0$. Using Lemma 4.3, let $\hat{\varphi}_N$ be the minimizer on the left-hand side of (4.7), and let $\varphi_N = \hat{\varphi}_N + \frac{1}{4\pi}\langle \psi - \hat{\varphi}_N \rangle$. Then $\langle \varphi_N \rangle = \langle \psi \rangle > 0$, and

$$\|\psi - \varphi_N\|_{L^\infty} \leq \|\psi - \hat{\varphi}_N\|_{L^\infty} + \frac{1}{4\pi}\langle |\psi - \hat{\varphi}_N| \rangle \leq 2\|\psi - \hat{\varphi}_N\|_{L^\infty} \leq 2A_2(q)N^{-q}\|\psi\|_{C^q}\,. \tag{4.10}$$

We now modify φ_N to generate a non-negative polynomial that still approximates ψ well. Let $\bar{c}_N = -\min\{\min_{\Omega \in \mathbb{S}^2} \varphi_N(\Omega), 0\} \geq 0$. Then by definition, $\varphi_N + \bar{c}_N$ is non-negative, and $\langle \varphi_N + \bar{c}_N \rangle$ is positive. Hence the function

$$\varphi_N^+ := \frac{\langle \varphi_N \rangle}{\langle \varphi_N + \bar{c}_N \rangle}(\varphi_N + \bar{c}_N) = \frac{\langle \psi \rangle}{\langle \psi + \bar{c}_N \rangle}(\varphi_N + \bar{c}_N) \tag{4.11}$$

is a well-defined, non-negative polynomial on $\mathbb{S}^2$, and $\langle \varphi_N^+ \rangle = \langle \varphi_N \rangle = \langle \psi \rangle$. Moreover,

$$\|\varphi_N - \varphi_N^+\|_{L^2} = \frac{\|\langle \bar{c}_N \rangle \varphi_N - \langle \psi \rangle \bar{c}_N\|_{L^2}}{\langle \psi + \bar{c}_N \rangle} = \frac{4\pi \bar{c}_N \sqrt{\langle \varphi_N^2 \rangle - \frac{\langle \psi \rangle^2}{4\pi}}}{\langle \psi \rangle + 4\pi \bar{c}_N} \leq 4\pi \bar{c}_N \frac{\|\varphi_N\|_{L^2}}{\langle \psi \rangle}\,. \tag{4.12}$$

By Hölder's inequality, $\|\varphi_N\|_{L^2} \leq \sqrt{4\pi}\|\varphi_N\|_{L^\infty}$. Using triangle inequality, (4.10), and the fact that $\hat{\varphi}_N$ is the minimizer, we have

$$\|\varphi_N\|_{L^\infty} \leq \|\psi\|_{L^\infty} + \|\psi - \varphi_N\|_{L^\infty} \leq \|\psi\|_{L^\infty} + 2\|\psi - \hat{\varphi}_N\|_{L^\infty} \leq 3\|\psi\|_{L^\infty}\,. \tag{4.13}$$

Applying Hölder's inequality and substituting the bound for $\|\varphi_N\|_{L^\infty}$ in (4.13) into (4.12) yield

$$\|\varphi_N - \varphi_N^+\|_{L^2} \leq \left(24\pi^{3/2}\frac{\|\psi\|_{L^\infty}}{\|\psi\|_{L^1}}\right)\bar{c}_N \leq 24\pi^{3/2} M \bar{c}_N\,, \tag{4.14}$$

where the second inequality comes from the assumption that $\psi \in \mathcal{D}_M$. This bound will be used below in (4.18).

By construction, the vector of expansion coefficients for φ_N^+ is a feasible point of (3.2). Because the corresponding vector of expansion coefficients for $\mathcal{E}_{\mathrm{FP}_N^+}$ solves (3.2), we have

$$\|\mathcal{E}_{\mathrm{FP}_N} - \mathcal{E}_{\mathrm{FP}_N^+}\|_{L^2} \leq \|\mathcal{E}_{\mathrm{FP}_N} - \varphi_N^+\|_{L^2}. \tag{4.15}$$

Hence,

$$\begin{aligned}
\|\psi - \mathcal{E}_{\mathrm{FP}_N^+}\|_{L^2} &\leq \|\psi - \mathcal{E}_{\mathrm{FP}_N}\|_{L^2} + \|\mathcal{E}_{\mathrm{FP}_N} - \mathcal{E}_{\mathrm{FP}_N^+}\|_{L^2} \\
&\leq \|\psi - \mathcal{E}_{\mathrm{FP}_N}\|_{L^2} + \|\mathcal{E}_{\mathrm{FP}_N} - \varphi_N^+\|_{L^2} \\
&\leq \|\psi - \mathcal{E}_{\mathrm{FP}_N}\|_{L^2} + \|\mathcal{E}_{\mathrm{FP}_N} - \psi\|_{L^2} + \|\psi - \varphi_N^+\|_{L^2} \\
&\leq 2\|\psi - \mathcal{E}_{\mathrm{FP}_N}\|_{L^2} + \|\psi - \varphi_N^+\|_{L^2}
\end{aligned} \tag{4.16}$$

We bound each of these terms separately. Lemma 4.2 and the fact that $\|\psi\|_{H^q} \leq A_3\|\psi\|_{C^q}$ for some constant A_3, gives a bound on the first term:

$$\|\psi - \mathcal{E}_{\mathrm{FP}_N}\|_{L^2} \leq A_1(q)N^{-s}\|\psi\|_{H^q} \leq A_1(q)A_3N^{-s}\|\psi\|_{C^q} . \tag{4.17}$$

For the second term, we apply the triangle inequality, Hölder's inequality, and (4.14). This gives

$$\|\psi - \varphi_N^+\|_{L^2} \leq \|\psi - \varphi_N\|_{L^2} + \|\varphi_N - \varphi_N^+\|_{L^2} \leq \sqrt{4\pi}\|\psi - \varphi_N\|_{L^\infty} + \left(24\pi^{3/2}M\right)\bar{c}_N. \tag{4.18}$$

Since $\psi \geq 0$, $\bar{c}_N \leq \|\psi - \varphi_N\|_{L^\infty}$. We substitute this bound into (4.18), combine terms in $\|\psi - \varphi_N\|_{L^\infty}$, and apply the bound in (4.10). This gives

$$\|\psi - \varphi_N^+\|_{L^2} \leq \left(\sqrt{4\pi} + 24\pi^{3/2}M\right)\|\psi - \varphi_N\|_{L^\infty} \leq A_4(q,M)N^{-q}\|\psi\|_{C^q} \tag{4.19}$$

where $A_4(q,M) = 2A_2(q)\left(\sqrt{4\pi} + 24\pi^{3/2}M\right)$. Finally, by substituting the bounds in (4.17) and (4.19) into (4.16), the claim (4.5) is proved, with $A(q,M) = 2A_1(q)A_3 + A_4(q,M)$ ∎

For comparison, the next theorem provides error estimates for the uniform damping (UD_N) approximation.

THEOREM 4.4. *For $M > 0$, let $\mathcal{D}_M = \{g \in L^2(\mathcal{S}) : \|g\|_{L^2(\mathcal{S})} \leq M\|g\|_{L^1(\mathcal{S})}\}$. Then, given a non-negative $\psi \in H^q(\mathcal{S}) \cap \mathcal{D}_M$, $q \geq 0$, $\epsilon > 0$, there exists a constant $B(q,M,\epsilon)$ such that,*

$$\|\psi - \mathcal{E}_{UD_N}[\mathbf{u}^N]\|_{L^2(\mathcal{S})} \leq B(q,M,\epsilon)N^{-(s-a-\epsilon)}\|\psi\|_{H^q(\mathcal{S})}, \quad \forall N \in \mathbb{N}\,, \tag{4.20}$$

where $\mathbf{u}^N \in \mathbb{R}^n$ consists of the moments of ψ up to order N, and $s = \min\{q,p\}$, with p the order of filter F in (2.10)*. The constant a depends on $\mathcal{S}$: when $\mathcal{S} = [-1,1]$, $a = 3/4$; when $\mathcal{S} = \mathbb{S}^2$, $a = 1$.*

The following lemma is used in the proof of Theorem 4.4.

LEMMA 4.5. *For every $q \geq 0$ and $\delta > 0$, there exist constants $B_1(q,\delta)$ and $B_2(q,\delta)$ such that, for all $\psi \in H^q([-1,1])$ and $N \in \mathbb{N}$,*

$$\|\psi - \mathcal{E}_{FP_N}[\mathbf{u}^N]\|_{L^\infty([-1,1])} \leq \|\psi - \mathcal{E}_{FP_N}[\mathbf{u}^N]\|_{H^{\frac{1}{2}+\delta}([-1,1])} \leq B_1(q,\delta)N^{-(s-\frac{3}{4}-\frac{3\delta}{2})}\|\psi\|_{H^q([-1,1])}, \tag{4.21}$$

and for all $\psi \in H^q(\mathbb{S}^2)$ and $N \in \mathbb{N}$,

$$\|\psi - \mathcal{E}_{FP_N}[\mathbf{u}^N]\|_{L^\infty(\mathbb{S}^2)} \leq \|\psi - \mathcal{E}_{FP_N}[\mathbf{u}^N]\|_{H^{1+\delta}(\mathbb{S}^2)} \leq B_2(q,\delta)N^{-(s-1-\delta)}\|\psi\|_{H^q(\mathbb{S}^2)}\,, \tag{4.22}$$

where $\mathbf{u}^N \in \mathbb{R}^n$ consists of the moments of ψ up to order N, and $s = \min\{q,p\}$, with p the filter order in (2.10).

The first inequalities in (4.21) and (4.22) are Sobolev embedding theorems that can be found in [38] and [19], respectively. The second inequalities can be found in [6, Theorem 2.2] and [21, Theorem 8.2], respectively.

Proof of Theorem 4.4. For convenience, we denote $\mathcal{E}_{\mathrm{FP}_N}[\mathbf{u}^N]$ and $\mathcal{E}_{\mathrm{UD}_N}[\mathbf{u}^N]$ as $\mathcal{E}_{\mathrm{FP}_N}$ and $\mathcal{E}_{\mathrm{UD}_N}$, respectively. By the triangle inequality,

$$\|\psi - \mathcal{E}_{\mathrm{UD}_N}\|_{L^2(\mathcal{S})} \leq \|\psi - \mathcal{E}_{\mathrm{FP}_N}\|_{L^2(\mathcal{S})} + \|\mathcal{E}_{\mathrm{FP}_N} - \mathcal{E}_{\mathrm{UD}_N}\|_{L^2(\mathcal{S})} . \tag{4.23}$$

The bound for the first term in (4.23) is given by (4.6) in Lemma 4.2. For the second term, we use the definition of $\mathcal{E}_{\mathrm{UD}_N}$ in (2.16) to compute (recalling that m_0 and c_N

are constant over $\mathcal{S}$)

$$\|\mathcal{E}_{\mathrm{FP}_N} - \mathcal{E}_{\mathrm{UD}_N}\|_{L^2(\mathcal{S})} = \frac{\|\langle m_0 c_N\rangle \mathcal{E}_{\mathrm{FP}_N} - \langle m_0\psi\rangle c_N\|_{L^2(\mathcal{S})}}{\langle m_0\psi\rangle + \langle m_0 c_N\rangle} = \frac{B_3 c_N \sqrt{\langle \mathcal{E}^2_{\mathrm{FP}_N}\rangle - \frac{\langle\psi\rangle}{B_3}}}{\langle\psi\rangle + \langle c_N\rangle}\,, \tag{4.24}$$

where $B_3 = \langle 1\rangle$. Because $\|\mathcal{E}_{\mathrm{FP}_N}\|_{L^2(\mathcal{S})} \le \|\mathcal{E}_{\mathrm{P}_N}\|_{L^2(\mathcal{S})} \le \|\psi\|_{L^2(\mathcal{S})}$ and $c_N \le \|\psi - \mathcal{E}_{\mathrm{FP}_N}\|_{L^\infty(\mathcal{S})}$, it follows from (4.24) and $\psi \in \mathcal{D}_M$ that

$$\|\mathcal{E}_{\mathrm{FP}_N} - \mathcal{E}_{\mathrm{UD}_N}\|_{L^2(\mathcal{S})} \le \frac{B_3 c_N \|\mathcal{E}_{\mathrm{FP}_N}\|_{L^2(\mathcal{S})}}{\langle\psi\rangle + \langle c_N\rangle} \le B_3 \frac{\|\psi\|_{L^2(\mathcal{S})}}{\|\psi\|_{L^1(\mathcal{S})}} c_N \le B_3 M \|\psi - \mathcal{E}_{\mathrm{FP}_N}\|_{L^\infty(\mathcal{S})}. \tag{4.25}$$

The bound for the second term in (4.23) is then obtained by applying either (4.21) or (4.22) in Lemma 4.5 on the right-hand side of (4.25). Finally, by bounding for both terms in (4.23), the claim (4.20) is proved, with

$$B(q, M, \epsilon) = \begin{cases} A_1(q) + B_1(q, 2\epsilon/3) B_3 M\,, & \text{when } \mathcal{S} = [-1, 1] \\ A_1(q) + B_2(q, \epsilon) B_3 M\,, & \text{when } \mathcal{S} = \mathbb{S}^2 \end{cases} \tag{4.26}$$

chosen to be the constant. ▯

REMARK 1. *The error estimate in* (4.20) *appears to be sharp for both choices of* $\mathcal{S}$*. This is illustrated in Tables 4.1 and 4.2 with Sobolev target functions in the next subsection.*

REMARK 2. *The fact that* ψ *may be zero on* $\mathcal{S}$ *is what limits the error estimates for both the* FP_N^+ *approximation (Theorem 4.1) and the* UD_N *approximation (Theorem 4.4). However, if* ψ *is strictly positive and* $\mathcal{E}_{FP_N}[\mathbf{u}^N]$ *converges to* ψ *uniformly, then one can prove that both* $\mathcal{E}_{FP_N^+}$ *and* $\mathcal{E}_{UD_N}$ *recover the optimal rate for the* FP_N *approximation. Indeed, uniform convergence to a strictly positive function implies that* $\mathcal{E}_{FP_N}[\mathbf{u}^N] > 0$ *for all* N *greater than some* $\tilde{N}$*. In this case,* $\mathcal{E}_{FP_N^+}[\mathbf{u}^N] = \mathcal{E}_{UD_N}[\mathbf{u}^N] = \mathcal{E}_{FP_N}[\mathbf{u}^N]$.

4.2. Convergence Tests. In this subsection, we present numerical convergence results for the FP_N^+ and UD_N approximations. These results suggest that the stronger assumptions for the FP_N^+ approximation about the underlying function (C^q vs. H^q) in Theorem 4.1 may not be necessary. Meanwhile, the convergence rates for the UD_N approximation in Theorem 4.4 appear to be sharp.

We begin with one-dimensional tests for functions defined on $[-1, 1]$. For an expansion of degree N, we use for $\mathcal{Q}$ (cf. (3.2)) a Gauss-Legendre quadrature rule with $N + 1$ points, which has degree of precision $2N + 1$. The observed convergence rates of the L^2 approximation errors for several functions on $[-1, 1]$, each with different regularity properties, are listed in Table 4.1. Corresponding results for the P_N and FP_N approximation are included for reference.

The target functions (except for the smooth function) are of the form

$$\psi(\mu) = \begin{cases} (\mu - \hat{\mu})^r, & \mu \in [\hat{\mu}, 1] \\ 0, & \mu \in [-1, \hat{\mu}) \end{cases}\,, \tag{4.27}$$

where r and $\hat{\mu}$ are regularity parameters. For $\hat{\mu} \in (-1, 1)$, the function (4.27) belongs to $H^q([-1, 1])$ for all $q < r + \frac{1}{2}$.

- ***Step function***: $(r, \hat{\mu}) = (0, 0.75)$. This function is in $H^q([-1, 1])$, $\forall q < 0.5$. From Table 4.1, it can be seen that the P_N^+ (FP_N^+ with no spectral filter) and FP_N^+ approximations converge roughly at the same rate as the P_N and FP_N approximation.

The UD_N approximations, on the other hand, have a slower convergence rate, which is consistent with result of Theorem 4.4. Note that $\hat{\mu}$ can be arbitrarily chosen from $(-1, 1)$. However, for some choices of $\hat{\mu}$, the approximation errors may converge faster than the (worst case) error estimates given in Theorems 4.1 and 4.4.

- ***Singular function***: $(r, \hat{\mu}) = (-0.1, 0.75)$. This function is an L^2 function with a singularity at $\mu = 0.75$. For this function, the UD_N approximation does not converge, while the FP_N^+ approximation still converges roughly at the same rate as the FP_N approximation.
- ***Smooth function***: $\psi(\mu) = \exp(5\mu \sin(10\mu))$. This function is in $C^\infty([-1, 1])$. Here we observe, as is expected from Theorems 4.1 and 4.4, that the FP_N^+ and UD_N approximations to converge with the order of the spectral filter used to define them. If no filter is applied, both approximations converge spectrally.
- ***Sobolev function***: $(r, \hat{\mu}) = (0.5, 0.975)$ and $(r, \hat{\mu}) = (3, 0.75)$. These functions belong to $H^q([-1, 1])$ for all $q < 1$ and for all $q < 3.5$, respectively. For such functions, the UD_N approximations typically converge at slower rates than the P_N and P_N^+ approximations. In the first case, we select $\hat{\mu} = 0.975$ in order to show that the estimate in Theorem 4.4 is most likely sharp. Indeed, as reported in Table 4.1, the convergence rate of the UD_N ansatz for this target function is around 0.25, which matches the error estimate provided in Theorem 4.4. In the second case, $r = 3$ is chosen to illustrate the effect of the spectral filters on the convergence rate. In the results shown in Table 4.1, we observe that a loss in order occurs for the UD_N approximation when $p > r + 1/2$—that is, when the order of the filter is greater than the regularity of ψ.

We next consider target functions Ψ on $\mathbb{S}^2$ that are simple extensions of functions ψ on $[-1, 1]$:

$$\Psi(\mu, \phi) := \psi(\mu), \quad \forall(\mu, \phi) \in [-1, 1] \times [0, 2\pi] \,. \tag{4.28}$$

Due to behavior at the poles of $\mathbb{S}^2$, these extensions may not have the same regularity on $\mathbb{S}^2$ as the original function does on $[-1, 1]$. However, because of the tensor product construction, we expect the same convergence rates. For approximations of degree N, we use for $\mathcal{Q}$ (cf. (3.2)) the product quadrature rule on $\mathbb{S}^2$ defined in Section 3.2.3, with degree of precision $2N + 1$. To ensure that our results do not depend on a special alignment of the quadrature with the coordinate axes, we rotate the points about the x_1 and x_2 axes by one and two radians, respectively.

The observed L^2 convergence rates for functions of the form (4.28) with ψ defined as in (4.27) are also listed in Table 4.1. We observe that, for most cases, the rates for the extended functions with rotated quadrature are close to the rates for the corresponding functions on $[-1, 1]$. Larger variations occur with the UD_N approximation, most noticeably for the singular function.

Finally, we consider general functions on $\mathbb{S}^2$. Convergence rates for these functions are presented in Table 4.2. In Table 4.2, the step function Ψ on $\mathbb{S}^2$ is defined as

$$\Psi(\mu, \phi) = \begin{cases} 1, & \Omega_1 \in [-0.2, 0.4], \Omega_2 \in [0.5, 0.9] \\ 0, & \text{otherwise} \end{cases}, \tag{4.29}$$

where $\Omega_1 = \sqrt{1 - \mu^2} \cos\phi$ and $\Omega_2 = \sqrt{1 - \mu^2} \sin\phi$. This function is in $H^q(\mathbb{S}^2)$ for all $q < 0.5$. The location of the support for Ψ can be arbitrarily chosen; some choices may lead to faster convergence rates. For this particular choice, we observe that the UD_N approximation does not converge (or does so very slowly), while the FP_N^+ approximation converges with rate ≈ 0.5, just as the FP_N approximation does.

Filter Order	Approx. Type	**Step** $q < 0.5$		**Singular** $q < 0.4$		**Smooth** $q = \infty$		**Sobolev** $q < 1$		**Sobolev** $q < 3.5$	
		[-1, 1]	$\mathbb{S}^2$	[-1, 1]	$\mathbb{S}^2$	[-1, 1]	$\mathbb{S}^2$	[-1, 1]	$\mathbb{S}^2$	[-1, 1]	$\mathbb{S}^2$
No filter	P_N	0.49	0.51	0.53	0.50	∞	∞	0.97	1.33	3.49	3.47
	UD_N	0.08	0.06	-0.04	-0.22	∞	∞	0.21	0.06	3.09	2.92
	P_N^+	0.51	0.51	0.51	0.49	∞	∞	1.02	1.15	3.52	3.49
$p = 2$	FP_N	0.49	0.51	0.52	0.50	1.99	1.95	0.97	1.32	1.99	1.96
	UD_N	0.09	0.10	-0.02	-0.23	1.99	1.95	0.25	0.05	2.03	2.20
	FP_N^+	0.51	0.51	0.51	0.49	1.99	1.95	1.02	1.15	1.99	1.96
$p = 4$	FP_N	0.49	0.50	0.52	0.49	3.98	3.90	0.97	1.27	3.47	3.43
	UD_N	0.07	0.15	-0.05	-0.19	3.98	3.89	0.26	0.08	3.02	2.77
	FP_N^+	0.51	0.51	0.51	0.48	3.98	3.90	1.01	1.15	3.53	3.61
$p = 6$	FP_N	0.49	0.47	0.44	0.40	5.96	5.84	0.98	1.07	3.47	3.41
	UD_N	0.10	0.23	0.05	0.00	5.96	5.81	0.18	0.11	3.04	2.86
	FP_N^+	0.49	0.47	0.45	0.41	5.96	5.81	0.97	1.05	3.42	3.39

Table 4.1: Convergence Rates – The observed L^2 convergence rates for the P_N, FP_N, UD_N, and FP_N^+ approximations to target functions on $[-1, 1]$ listed in Section 4.2 and and their extensions on $\mathbb{S}^2$ defined in (4.28). Note that the index q express the regularity of the target functions on $[-1, 1]$.

Filter Order	Approx. Type	**Step** (4.29)	**Sobolev** (4.30)	Filter Order	Approx. Type	**Step** (4.29)	**Sobolev** (4.30)
No filter	P_N	0.51	1.87	$p = 4$	P_N	0.50	1.73
	UD_N	0.02	1.07		UD_N	0.07	1.10
	P_N^+	0.52	1.81		P_N^+	0.52	1.71
$p = 2$	P_N	0.50	1.83	$p = 6$	P_N	0.45	1.37
	UD_N	0.04	1.18		UD_N	0.07	1.14
	P_N^+	0.52	1.78		P_N^+	0.46	1.36

Table 4.2: Convergence Rates – The observed L^2 convergence rates for the P_N, FP_N, UD_N, and FP_N^+ approximations to functions defined in (4.29) and (4.30).

The next target function is a Sobolev function on $\mathbb{S}^2$, which is given by

$$\Psi(\mu, \phi) = \psi_1(\mu)\psi_2(\phi), \tag{4.30}$$

where

$$\psi_1(\mu) = \begin{cases} 0.25, & |\mu| \in [0, 0.25) \\ 0.5 - |\mu|, & |\mu| \in [0.25, 0.5) \\ 0, & \text{otherwise} \end{cases}, \psi_2(\phi) = \begin{cases} 0.25\pi, & |\phi| \in [0, 0.25\pi) \\ 0.5\pi - |\phi|, & |\phi| \in [0.25\pi, 0.5\pi) \\ 0, & \text{otherwise} \end{cases}, \tag{4.31}$$

respectively. This function Ψ is in $H^q(\mathbb{S}^2)$, for all $q < 2$. The convergence rate of the UD_N approximation is near one, as predicted by the error estimate given in Theorem 4.4. Hence, (4.20) appears to be a sharp error estimate for the UD_N approximation. The FP_N^+ approximation still converges at roughly the same rate as the FP_N approximation.

REMARK 3. *In all the convergence tests we performed, the FP_N^+ approximation always converges at roughly the same rate as the FP_N approximation, even if the continuity assumption in Theorem 4.1 is violated, i.e., the target function belongs to H^q, but not to C^q.*

5. Numerical Results on Line Source Benchmark Problem. In this section, we present solutions of the line source problem using the FP_N^+ closure and compare them to the results using P_N, FP_N, and PP_N closures (cf. Sections 2.2, 2.3, 2.4). Similar results for P_N, FP_N, and PP_N can be found in [4], [42] and [18], respectively. Results from the UD_N closure (cf. Section 2.5) are also included in the comparison.

5.1. The line source benchmark. The line source benchmark problem was first formulated in [16], along with an exact solution. Since then, it has been used to study the behavior of various angular approximations for linear kinetic equations [4, 23, 34, 42]. It is a notoriously difficult problem that provides insight into the strengths and weaknesses of different approximations and how to pursue improvements.

The problem is as follows: An initial pulse of particles are distributed isotropically along an infinite line in space and move through an infinite material medium with constant scattering cross-section. If this line is aligned with the x_3-axis, then f does not depend on x_3 and the transport equation (2.1) reduces to

$$\partial_t f + \xi \partial_{x_1} f + \eta \partial_{x_2} f = \frac{\sigma}{4\pi} \langle f \rangle - \sigma f \tag{5.1}$$

with initial condition $f^{\mathrm{in}}(x, \Omega) = \frac{1}{4\pi} \delta(x_1, x_2)$.

5.2. Numerical results. We simulate the line source problem with $\sigma = 1.0$. A steep Gaussian distribution with variance $\varsigma^2 = 9 \times 10^{-4}$ is used to approximate the delta function initial condition, and a small positive floor is added:

$$f^{\mathrm{in}}(x, \Omega) \approx \frac{1}{4\pi} \left(\max \left(\frac{1}{2\pi\varsigma^2} e^{\frac{-(x_1^2 + x_2^2)}{2\varsigma^2}}, f_{\mathrm{floor}} \right) \right) . \tag{5.2}$$

The floor is only needed for the PP_N closure, which requires a strictly positive distribution. For our calculations, we set $f_{\mathrm{floor}} = 10^{-4}$. We truncate the infinite spatial domain to a $[-1.5, 1.5] \times [-1.5, 1.5]$ square centered at the origin and impose artificial boundary condition equal to f_{floor}. The computation is run to a final time $t_{\mathrm{final}} = 1.0$.

The calculations are performed using a 200×200 mesh, hence each square spatial cell has side length $h = 0.015$. The time step for the P_N and FP_N methods is $\Delta t = 0.45h$; for the UD_N, PP_N, and FP_N^+ methods is $\Delta t = 0.225h$ and a minmod-type slope limiter is used to enforce positivity in the kinetic scheme. See the supplementary materials for details. The more restrictive step is used to maintain positivity of the particle concentration for the FP_N^+, UD_N, and PP_N closures.

The optimization algorithm used to solve (3.5) is presented in the supplementary materials.

In Figures 5.1 and 5.2, we plot the particle concentration $\rho = \langle f \rangle$ for various methods with moments of order $N = 11$ and quadrature precision of degree $N_{\mathcal{Q}} = 2N + 1 = 23$ (the minimum required precision) and $N_{\mathcal{Q}} = 47$. We consider both product and Lebedev quadrature rules defined in Section 3.2.3. Figure 5.1 shows the heat maps over the entire two-dimensional domain and Figure 5.2 presents the one-dimensional line-outs along the x_1-axis. For comparison, the exact transport solution is included in all the line-out figures.

We observe the following qualitative features from the numerical results:

- P_N (Figures 5.1(b), 5.2(b)) The P_N method clearly suffers from severe oscillations that lead to particle concentrations with large negative values. The P_N solution preserves the rotational invariance of the exact line source solution and the quadrature has minimal effect on the P_N solution, as long as it has degree of precision $2N + 1$.

- FP_N (Figures 5.1(c), 5.2(c)) The FP_N solution contains only mild oscillations. Like the P_N method, the FP_N method maintains rotational invariance in the solution. However, it still suffers from the loss of positivity in the particle concentration, as can be seen near the wave front. Like the P_N solution, the FP_N solution is unaffected by the degree of quadrature precision $N_{\mathcal{Q}}$, as long as $N_{\mathcal{Q}} \geq 2N+1$.
- PP_N (Figures 5.1(d), 5.1(g), 5.2(d), 5.2(g)) Oscillations still occur in the PP_N solution. However, they are much weaker than those occurring in the P_N solution. Because the PP_N closure uses a positive ansatz, the PP_N solution maintains positivity in the particle concentration. However, because the ansatz is not polynomial, its moments cannot be evaluated exactly with a numerical quadrature rule. As a consequence, the PP_N solution loses rotational invariance and suffers from ray effects. Moreover, the accuracy of the PP_N solution is highly dependent on the quadrature precision.
- UD_N (Figures 5.1(e), 5.1(h), 5.2(e), 5.2(h)) The UD_N closure imposes strong damping which effectively removes all oscillations from the solution. The closure also maintains a positive particle concentration. However, the damping has a significant effect on accuracy; indeed, the UD_N solution completely misses the location of the wave front.
- FP_N^+ (Figures 5.1(f), 5.1(i), 5.2(f), 5.2(i)) As expected, the FP_N^+ solution preserves the positivity of the particle concentration. It contains only tiny oscillations that are barely visible in the figures, which indicates that the nonlinear filter (constrained optimization) in the FP_N^+ method not only maintains the positivity of the ansatz, but also slightly damps the oscillations. This damping does reduce the accuracy of the solution near the origin, when compared to the FP_N results. Like the P_N and FP_N solutions, the FP_N^+ solution is also rotationally invariant. The accuracy of the FP_N^+ solution is slightly improved by using quadrature with a higher degree of precision. However, the computational cost of solving problem (3.2) may become prohibitive. (See Table 5.1 in Section 5.3 below.)

Remark 4 (Lebedev Quadrature). *The Lebedev quadrature [26] requires fewer quadrature points than the product quadrature (see Section 3.2.3) does to achieve the same degree of precision. For comparison, we test the* FP_N^+ *closure with Lebedev quadrature rules that have degree of precision* $N_{\mathcal{Q}} = 23$ *and* $N_{\mathcal{Q}} = 47$ *on the line source problem, and the solutions are shown in Figures 5.1(j), 5.1(k), and 5.2(j), 5.2(k). With the Lebedev rule, the computation time is reduced by about* 25%*, due to the fewer number of constraints in optimization problem, as shown in Table 5.1.*

Remark 5 (Location of "hard" problems). *In the numerical tests, we observed that most of the computation time of the* FP_N^+ *method is spent in solving the "hard" optimization problems that occur near the wave front, as seen in Figure 5.3 for quadrature precision* $N_{\mathcal{Q}} = 23$ *and* $N_{\mathcal{Q}} = 47$.

5.3. Computational performance. In Table 5.1, we list the computation times for the line source calculations in Section 5.2. The P_N and FP_N methods are significantly faster because they (i) can take larger time steps, since positivity does not need to be enforced; (ii) have simpler flux evaluations; and (iii) most importantly, require no numerical optimization for their closure. The UD_N method has the least computation cost among all positive-preserving methods (UD_N, PP_N, FP_N^+), but still takes about twice the time of the P_N and FP_N methods. The PP_N method is by far the slowest. The computation time for the FP_N^+ method depends heavily on the type of optimization algorithm and the number of quadrature points. For $N_{\mathcal{Q}} = 47$, constraint reduction (CR) reduces the computation time for the FP_N^+ method by about a factor of two. For $N_{\mathcal{Q}} = 23$, the benefit of CR is less significant ($10 \sim 30\%$), as the number of constraints in the optimization problem is lower. In addition, our extended version of Mehrotra's Predictor-Corrector (MPC) algorithm clearly outperforms the affine-scaling (AS) algorithm, with or without CR. The computation time using the Lebedev quadrature with degree of precision 23 and 47 is also reported in Table 5.1. As discussed in Remark 4, the Lebedev quadrature rule requires fewer points to reach the same degree of precision than the product quadrature, leading to lower computation time. Overall the best algorithm is MPC/CR with the Lebedev quadrature. With degree of precision $N_{\mathcal{Q}} = 23$ (the minimum required), the computation time is about ten times that of the UD_N closure. In the next subsection, we compare efficiency of these methods, taking into account accuracy.

Quadrature Type **Degree** **# of points**	Product $N_{\mathcal{Q}} = 23$ $\lvert\mathcal{Q}\rvert = 144$	Product $N_{\mathcal{Q}} = 47$ $\lvert\mathcal{Q}\rvert = 576$	Lebedev $N_{\mathcal{Q}} = 23$ $\lvert\mathcal{Q}\rvert = 105$	Lebedev $N_{\mathcal{Q}} = 47$ $\lvert\mathcal{Q}\rvert = 401$
P_{11}	270	286	—	—
FP_{11}	272	287	—	—
UD_{11}	448	1732	—	—
PP_{11}	13798	49574	—	—
FP_{11}^{+} (AS)	7726	32941	6212	22092
FP_{11}^{+} (MPC)	6600	27319	5192	16925
FP_{11}^{+} (AS/CR)	5731	16277	4383	11537
FP_{11}^{+} (MPC/CR)	5929	12925	4336	8877

Table 5.1: The computation times (sec) for the line source benchmark with various closures with $N = 11$. The optimization problems in the FP_N^+ closure are solved by the algorithms described in the supplementary materials, including affine-scaling (AS), Mehrotra's predictor-corrector (MPC), and their constraint-reduced (CR) variants.

5.4. Efficiency. The ultimate goal in the development of the FP_N^+ closure is to generate an approximate solution of the transport equation that is accurate, preserves positivity of the particle concentration, and is efficient for challenging test problems when the underlying solution lacks high regularity. To this end, we compare the efficiency of the FP_N^+ and UD_N closures by examining the cost and accuracy of solving the line source benchmark for different values of the moment order N. To allow for larger values of N, we use a smoother initial condition (a Gaussian distribution, as in (5.2), with variance $\varsigma^2 = 10^{-2}$), reduce the spatial mesh from 200×200 cells to 100×100 cells, and use only quadrature rules with $N_{\mathcal{Q}} = 2N + 1$ (the minimum required degree of precision). All other parameter values are identical to those listed in Section 5.2.

Figure 5.4 illustrates the efficiency comparison between the UD_N and FP_N^+ closures, the latter implemented with the MPC/CR optimization algorithm. The FP_N^+ closure is tested on both the product and Lebedev quadrature. We plot the spatial errors

$$E_{\mathrm{FP}_N^+} := \|\rho_{\mathrm{exact}} - \rho_{\mathrm{FP}_N^+}\|_{L^2(\mathbb{R}^2)} \quad \text{and} \quad E_{\mathrm{UD}_N} := \|\rho_{\mathrm{exact}} - \rho_{\mathrm{UD}_N}\|_{L^2(\mathbb{R}^2)}, \tag{5.3}$$

versus the computation time. Here ρ_{exact}, $\rho_{\mathrm{FP}_N^+}$, and ρ_{UD_N} are the particle concentration at t_{final} of the exact, FP_N^+, and UD_N solutions, respectively. Each data point in Figure 5.4 represents a solution of the moment equations and is marked with a number that corresponds to the value of N. The data shows that, except for very low orders, the FP_N^+ solutions are two to ten times faster than the UD_N solutions to reach the same accuracy.

5.5. Space-Time Convergence. In this subsection, we compute space-time convergence rates of the second-order kinetic scheme used in the solution of (2.4) (see [2] and the supplementary materials for details) when using the UD_N and FP_N^+ closures. Convergence rates when using the FP_N closure are also included for reference. In the numerical tests reported in this section, the spectral filter is implemented in the filtered equation (2.12), and the FP_N, UD_N, and FP_N^+ closures are defined based on the moments $\mathbf{u}^*$ in (2.12). By doing so, we eliminate the influence of the spectral filter on the convergence properties of the numerical scheme (see [15]), so that the numerical results reflect only the effect of enforcing positivity in the UD_N and FP_N^+ closures.[10]

As before, we truncate the spatial domain to a $[-1.5, 1.5] \times [-1.5, 1.5]$ square centered at the origin and impose artificial boundary condition equal to $\rho_{\text{floor}} = 10^{-4}$. The computation is run to a final time $t_{\text{final}} = 1.0$. The numerical scheme is tested with initial condition on the particle concentration

$$\rho^{\text{in}}(x) = \begin{cases} \cos^5(2\sqrt{x_1^2 + x_2^2}), & \text{if } 2\sqrt{x_1^2 + x_2^2} \le \frac{\pi}{2}, \\ \rho_{\text{floor}}, & \text{otherwise,} \end{cases} \quad . \tag{5.4}$$

For $N > 0$, all moments are initially set to zero. All parameter values we used were identical to those listed in Section 5.2, except that the moment order N is chosen to be 5 and 7, instead of 11.

Since an analytic solution is not available in our problem, we define the space-time error E_h^p by

$$E_h^p := \|\mathbf{u}_h - \mathbf{u}_{h/2}\|_{L^p(\mathbb{R}^2, L^2(\mathbb{R}^n))}\ , \tag{5.5}$$

where $\mathbf{u}_h(x) \in \mathbb{R}^n$ is the computed solution to the moment equation with the finite volume scheme at $t_{\text{final}} = 1$, h denotes the side length of the square spatial cells, and the norm is defined as $\|\mathbf{v}\|_{L^p(\mathbb{R}^2, L^2(\mathbb{R}^n))} := \left(\int_{\mathbb{R}^2} \|\mathbf{v}(x)\|_2^p dx\right)^{1/p}$ for $p < \infty$, and $\|\mathbf{v}\|_{L^\infty(\mathbb{R}^2, L^2(\mathbb{R}^n))} := \max_{x \in \mathbb{R}^2} \|\mathbf{v}(x)\|_2$ for $p = \infty$.

Table 5.2 reports the space-time errors and observed convergence rates for FP_N, UD_N, and FP_N^+ closures with $p = 1$ and $p = \infty$ for moment order $N = 5$ and $N = 7$. The observed convergence rate ν is computed by

$$\nu := \log\left(\frac{E_{h_i}^p}{E_{h_{i+1}}^p}\right) \log\left(\frac{h_i}{h_{i+1}}\right)^{-1}, \quad i = 1, \ldots, 4, \tag{5.6}$$

where h_i is the side length of spatial cells defined by the square meshes listed in the first column of Table 5.2.[11] The results in Table 5.2 indicate that the expected rate $\nu \approx 2$ is achieved by the FP_N and FP_N^+ closures[12], while the UD_N closure causes a serious degradation in the convergence order.

[10] We referred to this in Section 2.3 as the *continuous embedding* of the filter. With it, we expect (and observe) second-order space-time accuracy for the FP_N closure, whereas for the *discrete embedding* approach that applies the filter at each time step, we expect (and observe) only first-order accuracy in time.

[11] The time step Δt is also refined in such a way that the ratio $\Delta t/h$ stays fixed.

[12] The only noticeable difference is the convergence rate for E_h^∞ with $N = 5$ on the 320^2 mesh.

	FP_5		UD_5		FP_5^+		FP_7		UD_7		FP_7^+	
mesh	E_h^1	ν	E_h^1	ν	E_h^1	ν	E_h^1	ν	E_h^1	ν	E_h^1	ν
20^2	4.9e-3	—	1.5e-2	—	5.7e-3	—	5.8e-3	—	1.4e-2	—	6.2e-3	—
40^2	1.48e-3	1.7	1.4e-3	3.4	1.3e-3	2.1	1.8e-3	1.7	1.7e-3	3.0	1.6e-3	2.0
80^2	3.7e-4	2.0	6.9e-4	1.1	3.6e-4	1.9	4.4e-4	2.0	7.7e-4	1.2	4.3e-4	1.9
160^2	8.9e-5	2.0	1.3e-3	-0.9	8.7e-5	2.1	1.1e-4	2.0	8.6e-4	-0.2	1.0e-4	2.1
320^2	2.2e-5	2.0	2.6e-3	-1.0	2.2e-5	2.0	—	—	—	—	—	—
	E_h^∞	ν	E_h^∞	ν	E_h^∞	ν	E_h^∞	ν	E_h^∞	ν	E_h^∞	ν
20^2	1.1e-2	—	4.7e-2	—	1.7e-2	—	1.2e-2	—	4.4e-2	—	1.6e-2	—
40^2	4.0e-3	1.5	6.0e-3	3.0	5.0e-3	1.8	4.3e-3	1.5	7.2e-3	2.6	5.1e-3	1.7
80^2	1.0e-3	1.9	7.2e-3	-0.3	1.2e-3	2.0	1.1e-3	1.9	9.0e-3	-0.3	1.1e-3	2.2
160^2	2.5e-4	2.0	2.3e-2	-1.7	2.7e-4	2.2	2.8e-4	2.0	2.0e-2	-1.1	2.8e-4	2.0
320^2	6.2e-5	2.0	3.9e-2	-0.8	8.0e-5	1.8	—	—	—	—	—	—

Table 5.2: Convergence of space-time errors with $p = 1$ and $p = \infty$ for FP_N, UD_N, and FP_N^+ closures. The results for moment orders $N = 5$ and $N = 7$ are reported. The spatial mesh sizes are listed in the first column. In order to minimize the influence of the optimization tolerance in the FP_N^+ method, the tolerance ε is set to 10^{-8}.

6. Conclusion and Discussion. We have presented a new moment closure, the FP_N^+ closure, for generating approximate solutions of the transport equation. The new closure is based on the solution of an optimization problem that modifies the coefficients in the filtered spherical harmonic expansion by enforcing positivity on a properly chosen quadrature set.

We have proven that for target functions in the space C^q, where $q \geq 0$ is an integer, the FP_N^+ approximation converges in L^2 at the same rate as the FP_N approximation. However, the necessity of this assumption was not observed in the numerical results; indeed for several target functions in $H^q \setminus C^q$, we observe that the two approximations still converge at the same rate. For some special cases (not discussed in this paper), we are able to prove this fact. However, a general result is the subject of future work.

We have also investigated a simpler closure, which we refer to as the UD_N closure, that is based on a spatial limiter developed in [32] for finite volume schemes. For functions in H^q, we prove suboptimal convergence rates for the UD_N approximation. Based on numerical tests, we believe that these rates are sharp. For problems with less regularity, we expect that the additional accuracy of the FP_N^+ closure will outweigh the additional cost, when compared to the UD_N approach. Our simulation results support this conjecture in the case of the line source benchmark. They also show that the UD_N closure degrades the space-time convergence rate of the PDE solver for the moment equations. For the FP_N^+ closure, we observe minimal, if any, effect. For more regular problems, we expect the accuracy of the two closures to be comparable. In fact, we have observed this for other test problem results not reported here. For these problems, the UD_N closure may be more efficient, and a more careful comparison will be performed in later work.

The optimization problem which defines the FP_N^+ closure requires a numerical solution; there are a variety of algorithms to do this. Here we have focused on interior-point algorithms. Because the main cost (per iteration) of these algorithms is proportional to the number of constraints, it is important to choose a quadrature rule that uses a small number of quadrature points while still maintaining the necessary degree of precision. Of the four algorithms tested, the new Mehrotra's Predictor-Corrector

(MPC) algorithm with the constraint reduction (CR) technique is the most efficient for the line source benchmark.

This paper has focused on the properties of the FP_N^+ approximation and also the efficiency of the optimization algorithm for (3.2). Future work will focus on improving the efficiency of the PDE solver used to integrate the moment equations. The current solver was designed for a general positive ansatz and enforces positivity at the kinetic level—that is, at every point in the quadrature set $\mathcal{Q}$. (Again, refer to the supplementary materials for details.) However, the simple polynomial form of the FP_N^+ approximation opens the possibility for a cheaper solver that still preserve positivity of the particle concentration and is also accurate and stable when the cross-section σ is very large, so that the particle transport becomes diffusive [25]. The current solver requires $\Delta t = \Delta x = O(\sigma^{-1})$ for accuracy and stability. Furthermore, the final time of interest typically scales linearly with σ. See [2] and citations therein for more details.

REFERENCES

[1] G. W. Alldredge, C. D. Hauck, D. P. O'Leary, and A. L. Tits, *High-order entropy-based moment closures: A computational study of the optimization problem.* Poster at DOE Applied Mathematics Program Meeting, 2011.

[2] G. W. Alldredge, C. D. Hauck, and A. L. Tits, *High-order entropy-based closures for linear transport in slab geometry II: A computational study of the optimization problem*, SIAM J. Sci. Comput., 34 (2012), pp. B361–B391.

[3] K. Atkinson, *Numerical integration on the sphere*, J. Austral. Math. Soc. Ser. B, 23 (1982), pp. 332–347.

[4] T. A. Brunner, *Forms of approximate radiation transport*, Tech. Report SAND2002-1778, Sandia National Laboratories, 2002.

[5] T. A. Brunner and J. P. Holloway, *One-dimensional Riemann solvers and the maximum entropy closure*, J. Quant Spect. and Radiative Trans, 69 (2001), pp. 543 – 566.

[6] C. Canuto and A. Quarteroni, *Approximation results for orthogonal polynomials in Sobolev spaces*, Math. Comp., 38 (1982), pp. pp. 67–86.

[7] K. Case and P. Zweifel, *Linear Transport Theory*, Addison-Wesley, Reading, MA, 1967.

[8] C. Cercignani, *The Boltzmann Equation and its Applications*, vol. 67 of Applied Mathematical Sciences, Springer-Verlag, New York, 1988.

[9] C. Cercignani, R. Illner, and M. Pulvirenti, *The Mathematical Theory of Dilute Gases*, vol. 106 of Applied Mathematical Sciences, Springer-Verlag, New York, 1994.

[10] F. Dai and Y. Xu, *Polynomial approximation in Sobolev spaces on the unit sphere and the unit ball*, J. of Approx. Theory, 163 (2011), pp. 1400 – 1418.

[11] F. Dai and Y. Xu, *Approximation Theory and Harmonic Analysis on Spheres and Balls*, Springer Monographs in Mathematics, Springer New York, 2013.

[12] R. Dautray and J. L. Lions, *Mathematical analysis and numerical methods for science and technology, Volume 6: Evolution Problems II*, Spinger-Verlag, Berlin, 2000.

[13] R. A. DeVore and G. G. Lorentz, *Contructive Approximation*, Springer-Verlag, 1993.

[14] B. Dubroca and J.-L. Fuegas, *Étude théorique et numérique d'une hiérarchie de modèles aus moments pour le transfert radiatif*, C.R. Acad. Sci. Paris, I. 329 (1999), pp. 915–920.

[15] M. Frank, C. Hauck, and K. Kuepper, *Convergence of filtered spherical harmonic equations for radiation transport*, J. Approx. Theory, (2014). submitted.

[16] B. D. Ganapol, *Homogeneous infinite media time-dependent analytic benchmarks for X-TM transport methods development*, tech. report, Los Alamos National Laboratory, March 1999.

[17] C. K. Garrett, C. Hauck, and J. Hill, *Optimization and large scale computation of an entropy-based moment closure*, J. Comput. Phys., 302 (2015), pp. 573 – 590.

[18] C. K. Garrett and C. D. Hauck, *A comparison of moment closures for linear kinetic transport equations: the line source benchmark*, Transport Theory and Statistical Physics, 42 (2013), pp. 203 – 235.

[19] P. Garrett, *Harmonic analysis on spheres, II*, (2011). Available at `http://www.math.umn.edu/~garrett/m/mfms/notes_c/spheres_II.pdf`.

[20] D. Gottlieb, S. Gottlieb, and J. Hesthaven, *Spectral Methods for Time-Dependent Problems*, Cambridge University Press, New York, 2007.

[21] B. Guo, *Spectral Methods and Their Applications*, World Scientific, Singapore, 1998.

[22] C. D. Hauck, *High-order entropy-based closures for linear transport in slab geometry*, Comm. Math. Sci., 9 (2011).

[23] C. D. Hauck and R. G. McClarren, *Positive P_N closures*, SIAM J. Sci. Comput., 32 (2010), pp. 2603–2626.

[24] J.H. Jung, D.P. O'Leary, and A.L. Tits, *Adaptive constraint reduction for convex quadratic programming*, Comput. Optim. Appl., 51 (2012), pp. 125 – 157.

[25] E. W. Larsen and J. B. Keller, *Asymptotic solution of neutron transport problems for small mean free paths*, J. Math. Phys., 15 (1974), pp. 75–81.

[26] V.I. Lebedev, *Quadratures on a sphere*, Comput. Math. Math. Phys., 16 (1976), pp. 10–24.

[27] V.I. Lebedev, *Spherical quadrature formulas exact to orders 25–29*, Sib. Math. J., 18 (1977), pp. 99–107.

[28] V.I. Lebedev, *A quadrature formula for the sphere of 59th algebraic order of accuracy*, Russian Acad. Sci. Dokl. Math., 50 (1995), pp. 283–286.

[29] V.I. Lebedev and D.N. Laikov, *A quadrature formula for the sphere of the 131st algebraic order of accuracy*, in Doklady. Mathematics, vol. 59, MAIK Nauka/Interperiodica, 1999, pp. 477–481.

[30] V.I. Lebedev and A.L. Skorokhodov, *Quadrature formulas of orders 41, 47, and 53 for the sphere*, Russian Acad. Sci. Dokl. Math., 45 (1992), pp. 587–592.

[31] E. E. Lewis and Jr. W. F. Miller, *Computational Methods in Neutron Transport*, John Wiley and Sons, New York, 1984.

[32] X. D. Liu and S. Osher, *Nonoscillatory high order accurate self-similar maximum principle satisfying shock capturing schemes I*, SIAM J. Numer. Anal., 33 (1996), pp. pp. 760–779.

[33] P. A. Markowich, C. A. Ringhofer, and C. Schmeiser, *Semiconductor Equations*, Springer-Verlag, New York, 1990.

[34] R. G. McClarren and C. D. Hauck, *Robust and accurate filtered spherical harmonics expansions for radiative transfer*, J. Comput. Phys., 229 (2010), pp. 5597 – 5614.

[35] R. G. McClarren, J. P. Holloway, and T. A. Brunner, *On solutions to the P_N equations for thermal radiative transfer*, J. Comput. Phys., 227 (2008), pp. 2864–2885.

[36] S. Mehrotra, *On the implementation of a primal-dual interior point method*, SIAM J. Optim., 2 (1992), pp. 575–601.

[37] G. N. Minerbo, *Maximum entropy Eddington factors*, J. Quant. Spectrosc. Radiat. Transfer, 20 (1978), pp. 541–545.

[38] E. Di Nezza, G. Palatucci, and E. Valdinoci, *Hitchhiker's guide to the fractional Sobolev spaces*, Bulletin des Sciences Mathématiques, 136 (2012), pp. 521 – 573.

[39] G. L. Olson, *Second-order time evolution of P_N equations for radiation transport*, J. Comput. Phys., 228 (2009), pp. 3072–3083.

[40] G. C. Pomraning, *Radiation Hydrodynamics*, Pergamon Press, New York, 1973.

[41] A. Quarteroni, *Some results of Bernstein and Jackson type for polynomial approximation in L^p-spaces*, Jpn. J. Appl. Math., 1 (1984), pp. 173–181.

[42] D. Radice, E. Abdikamalov, L. Rezzolla, and C. D. Ott, *A new spherical harmonics scheme for multi-dimensional radiation transport I: Static matter configurations*, J. Comput. Phys., 242 (2013), pp. 648 – 669.

[43] W. Walters, *Use of the Chebyshev-Legendre quadrature set in discrete-ordinate codes*, Tech. Report LA-UR-87-3621, Los Alamos National Laboratory, 1987.

[44] L.B. Winternitz, S.O. Nicholls, A.L. Tits, and D.P. O'Leary, *A constraint-reduced variant of Mehrotra's predictor-corrector algorithm*, Comput. Optim. Appl., 51 (2012), pp. 1001 – 1036.

[45] S. J. Wright, *Primal-Dual Interior-Point Methods*, SIAM, 1997.

[46] X. Zhang and C.W. Shu, *On maximum-principle-satisfying high order schemes for scalar conservation laws*, J. Comput. Phys., 229 (2010), pp. 3091 – 3120.

[47] X. Zhang and C. W. Shu, *Maximum-principle-satisfying and positivity-preserving high-order schemes for conservation laws: survey and new developments*, Proc. Roy. Soc. London A: Math., Phys. and Eng. Sci., 467 (2011), pp. 2752–2776.

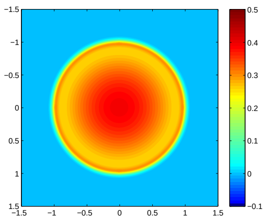

(a) Exact solution

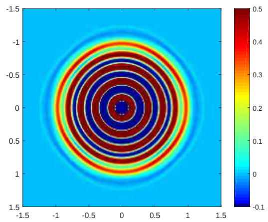

(b) P_{11}

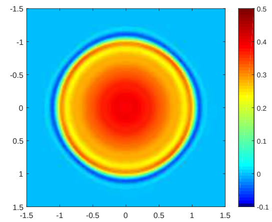

(c) FP_{11}

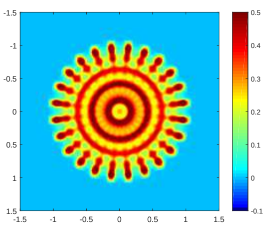

(d) PP_{11}, $N_{\mathcal{Q}} = 23$

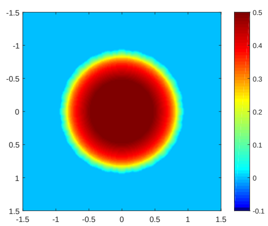

(e) UD_{11}, $N_{\mathcal{Q}} = 23$

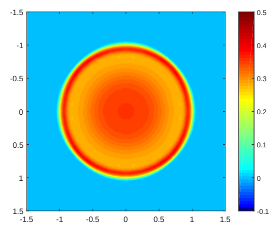

(f) FP_{11}^{+}, $N_{\mathcal{Q}} = 23$

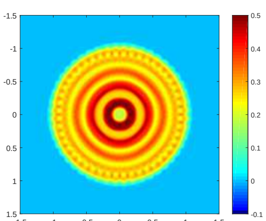

(g) PP_{11}, $N_{\mathcal{Q}} = 47$

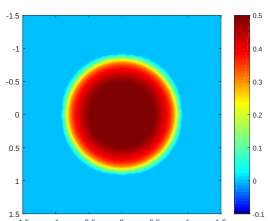

(h) UD_{11}, $N_{\mathcal{Q}} = 47$

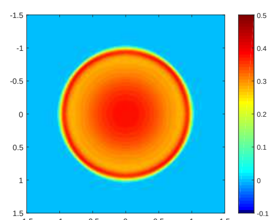

(i) FP_{11}^{+}, $N_{\mathcal{Q}} = 47$

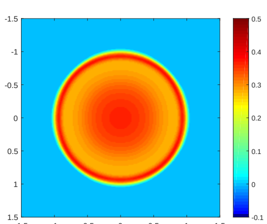

(j) FP_{11}^{+} (Lebedev, $N_{\mathcal{Q}} = 23$)

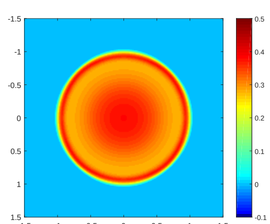

(k) FP_{11}^{+} (Lebedev, $N_{\mathcal{Q}} = 47$)

Fig. 5.1: Heat maps – the particle concentration $\rho = \langle f \rangle$ of the solutions to the line source benchmark for various methods.

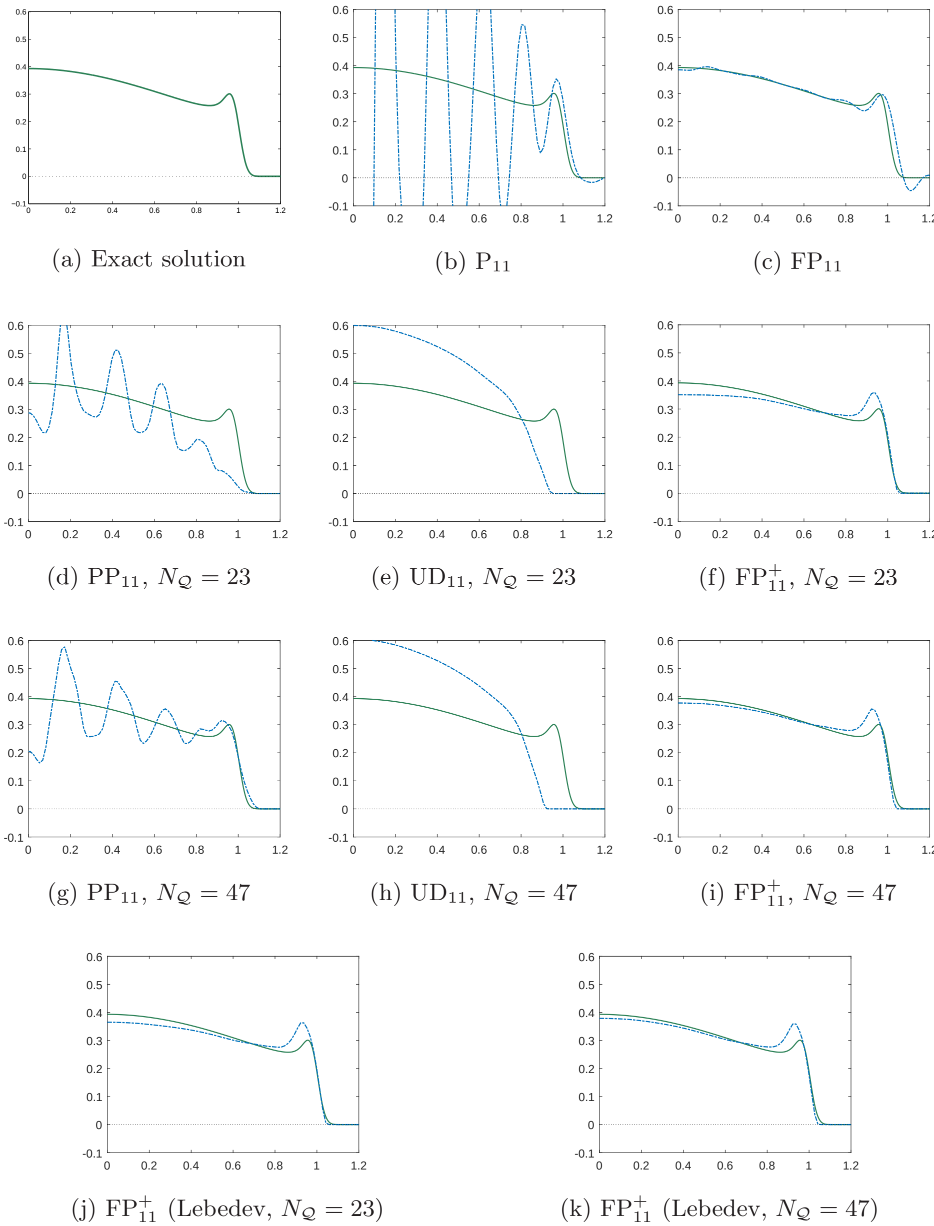

(a) Exact solution

(b) P_{11}

(c) FP_{11}

(d) PP_{11}, $N_{\mathcal{Q}} = 23$

(e) UD_{11}, $N_{\mathcal{Q}} = 23$

(f) FP^{+}_{11}, $N_{\mathcal{Q}} = 23$

(g) PP_{11}, $N_{\mathcal{Q}} = 47$

(h) UD_{11}, $N_{\mathcal{Q}} = 47$

(i) FP^{+}_{11}, $N_{\mathcal{Q}} = 47$

(j) FP^{+}_{11} (Lebedev, $N_{\mathcal{Q}} = 23$)

(k) FP^{+}_{11} (Lebedev, $N_{\mathcal{Q}} = 47$)

Fig. 5.2: Line-outs (along the x_1-axis) – the particle concentration $\rho = \langle f \rangle$ of the solutions to the line source benchmark for various methods.

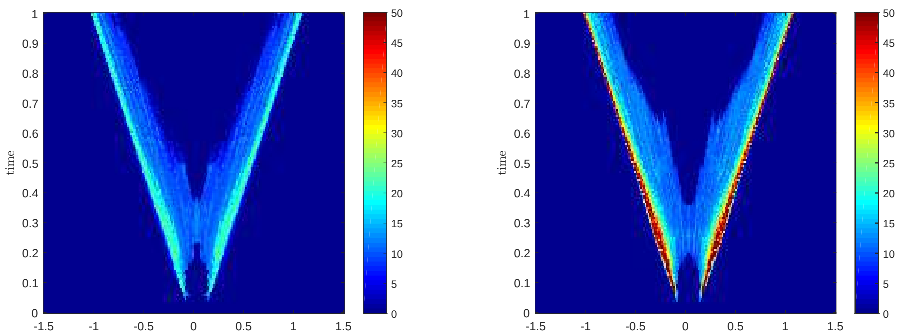

(a) $N_{\mathcal{Q}} = 23$ (b) $N_{\mathcal{Q}} = 47$

Fig. 5.3: The number of iterations needed to solve the optimization problem (3.5) for FP_{11}^{+} at each cell on the x_1-axis of the space and each time step.

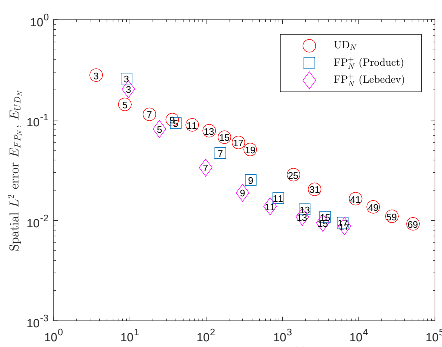

Fig. 5.4: Efficiency Comparison – Each data point on the figure represents a solution of the moment equations, and the x-axis and y-axis are respectively the computation time and spatial error for the solution. The integers inside each symbol are the moment orders N. The FP_N^{+} closure is implemented with the MPC/CR optimization algorithm.